GRHL2 enhances phosphorylated estrogen receptor DNA-binding and regulates ER-mediated transcriptional activation and repression

Running title: The role of GRHL2 in pS118-ER transcriptional activity

Rebecca M. Reese[a], Kyle T. Helzer[b], Kaelyn O. Allen[a], Christy Zheng[a], Natalia Solodin[a], Elaine T. Alarid[a]#

[a]McArdle Laboratory for Cancer Research, Department of Oncology and Carbone Comprehensive Cancer Center, University of Wisconsin – Madison, Madison WI

[b]Department of Human Oncology, University of Wisconsin – Madison, Madison WI

#Address correspondence to Elaine T. Alarid, alarid@oncology.wisc.edu

Data deposition: The data reported in this paper have been deposited in the Gene Expression Omnibus (GEO) database, www.ncbi.nlm.nih.gov/geo (accession number GSE202622).

Materials and Methods word count: 1996

Introduction, Results, Discussion word count: 3901

ABSTRACT

Phosphorylation of estrogen receptor α (ER) at serine 118 (pS118-ER) is induced by estrogen and is the most abundant post-translational mark associated with a transcriptionally active receptor. Cistromic analysis of pS118-ER from our group found enrichment of the GRHL2 motif near pS118-ER binding sites. In this report we use cistromic and transcriptomic analyses to interrogate the relationship between GRHL2 and pS118-ER. We found that GRHL2 is bound to chromatin at pS118-ER/GRHL2 co-occupancy sites prior to ligand treatment, and GRHL2 binding is required for maximal pS118-ER recruitment. pS118-ER/GRHL2 co-occupancy sites were enriched at active enhancers marked by H3K27ac and H3K4me1, along with FOXA1 and p300. Transcriptomic analysis yielded four subsets of ER/GRHL2 co-regulated genes revealing that GRHL2 can both enhance and antagonize E2-mediated ER transcriptional activity. Gene ontology analysis identified several coregulated genes involved in cell migration. Accordingly, knockdown of GRHL2 combined with estrogen treatment resulted in increased cell migration but no change in proliferation. These results support a model in which GRHL2 binds to select enhancers and facilitates pS118-ER recruitment to chromatin which then results in differential activation and repression of genes that control ER-positive breast cancer cell migration.

51 **INTRODUCTION**

52 Nuclear receptors are a class of transcription factors that modulate gene expression through DNA
53 interactions in response to stimuli such as steroid hormones. One such receptor is estrogen receptor α
54 (ER), which is expressed in over 70% of all breast cancers and is a major therapeutic target (1-3). ER
55 transcriptional activity is largely governed by the binding of its ligand, estrogen (E2), to the C-terminus of
56 the receptor (4, 5). Subsequently, the receptor binds to its consensus sequence, the estrogen response
57 element (ERE; 5'-GGTCAnnnTGACC-3') (6, 7), and interacts with other coregulators to modulate specific
58 gene expression (8-10).

59 ER transcriptional activity can be altered by a variety of post-translational modifications (PTMs),
60 including phosphorylation of several residues (11). Of particular note is phosphorylation of the serine 118
61 residue (pS118-ER) in the N-terminus of the receptor which can be induced in both a ligand-dependent
62 and independent manner (12, 13). Clinically, pS118-ER is associated with low grade, well-differentiated
63 breast tumors (14, 15). Mutational analysis assessing the function of pS118 has found the presence of
64 pS118 is required for maximal E2-mediated ER transcriptional activity (16-18). Our group recently
65 completed a genome-wide analysis of pS118-ER DNA-binding sites and found pS118-ER preferentially
66 binds enhancers marked by H3K27ac in breast cancer cells (19). In addition, motif analysis comparing sites
67 bound by pS118-ER and ER without pS118 identified enrichment of the GRHL2 motif (5'-AACCGGTT-3')
68 (20-23) near pS118-ER binding sites (19). GRHL2 is a member of the Grainyhead-like protein family (GRHL),
69 a class of transcription factors which regulate epithelial differentiation (24-34). GRHL2 has been
70 implicated in a number of cancers, demonstrating both tumor suppressive and oncogenic roles (35-54).
71 The genomic analysis of pS118-ER DNA binding provided early evidence of interplay between GRHL2 and
72 ER in breast cancer cells.

73 There is increasing evidence that GRHL2 plays a role in facilitating ER transcriptional activity.
74 GRHL2 was identified as an ER interactor in rapid immunoprecipitation mass spectrometry of endogenous

75 protein (RIME) studies (55), and this interaction increases upon estrogen treatment (56). Cistromic studies
76 of ER and GRHL2 found that 29-35% of ER binding sites are co-occupied by a GRHL2 binding site (57, 58),
77 indicating these two factors may function together to regulate gene transcription. Studies suggest that
78 GRHL2 acts through enhancer regions to facilitate the recruitment of MLL3, a lysine methyltransferase
79 responsible for depositing the enhancer marker H3K4me1 (58, 59). GRHL2 also co-occupies chromatin
80 with FOXA1, a pioneer factor associated with ER transcription, which promotes an open chromatin
81 structure and is found in regions marked by H3K4me1 (58, 60-63). GRHL2 chromatin-binding can also be
82 enhanced by E2 (19, 56) and E2-responsive GRHL2 binding sites are found more frequently in enhancer
83 regions identified by ER ChIA-Pet (56). Together with our work identifying the enrichment of the GRHL2
84 motif near pS118-ER binding sites, this evidence supports a role for co-regulation of gene expression by
85 GRHL2 and ER at enhancer regions. We also found pS118-ER preferentially binds near genes that are up-
86 regulated by E2, suggesting GRHL2 may co-activate genes with pS118-ER. However, GRHL2 can also
87 suppress the production of enhancer RNAs (eRNA) at ER enhancers for *GREB1*, *TFF1*, and *XBP1* (56),
88 indicating that GRHL2 is also capable of repressing ER transcriptional activity. The exact nature of the role
89 of GRHL2 in modulating ER transcriptional activity, more specifically pS118-ER transcriptional activity, and
90 the biological processes co-regulated by both factors are currently unclear.

91 In this report we examine the coordinate activities of GRHL2 and pS118-ER in the regulation of
92 gene expression in breast cancer cells using cistromic and transcriptomic approaches. Our data show
93 GRHL2 has a regulatory role in pS118-ER DNA binding at active enhancers, and GRHL2 can both activate
94 and repress pS118-ER target genes. We also found the combined activities of GRHL2 and pS118-ER control
95 the migratory behavior of breast cancer cells. These studies indicate a specific role for GRHL2 in
96 modulating pS118-ER transcriptional activity.

97 **MATERIALS AND METHODS**

98 **Cell culture**

99 MCF7, BT-474, SK-BR-3, MDA-MB-468, and MDA-MB-231 cells were maintained in 10% CO_2 at
100 37°C with high-glucose (4.5 g/L) Dulbecco's modified Eagles Medium (DMEM; Thermo Fisher, #11965092)
101 supplemented with 10% HyClone fetal bovine serum (FBS; Cytiva, #SH30910.03), 100 U/mL penicillin 100
102 ug/mL streptomycin (1% Pen/Strep; Gibco, #15140-122), and 1 mM sodium pyruvate (Gibco, #11360-070).
103 T47D and ZR-75-1 cells were maintained in Roswell Park Memorial Institute 1640 (RPMI; Thermo Fisher,
104 #11875-093) supplemented with 10% FBS and 1% Pen/Strep. BT-20 cells were maintained in Minimum
105 Essential Medium Alpha (MEMα; Thermo Fisher, #41061-029) supplemented with 10% FBS and 1%
106 Pen/Strep.

107 **Protein Preparation and Western Blot**

108 Protein samples were lysed in 1X Sample Buffer (62.5 mM Tris pH6.8, 2% SDS, 10% glycerol, 5%
109 β-mercaptoethanol) and subsequently boiled at 100°C for 10 minutes. Protein concentration for each
110 sample was quantified using the RC DC protein assay (Bio-Rad, #5000122) and 30-50 µg of protein were
111 run on a 10% SDS-PAGE gel. Proteins were transferred to a PVDF membrane (VWR, Cytiva, #10061-492),
112 blocked with 5% powdered milk in TBST (50 mM Tris-HCl pH7.4, 150 mM NaCl, 0.1% Tween-20), and
113 incubated overnight at 4°C in primary antibody. Primary antibodies used were ER (Santa Cruz
114 Biotechnology, #HC-20), pS118-ER (Abcam, #ab32396), GRHL1 (Santa Cruz Biotechnology, #sc-515541),
115 GRHL2 (Millipore Sigma, #HPA004820), GRHL3 (Santa Cruz Biotechnology, #sc-398838), β-actin (Millipore
116 Sigma, #A5441), and TBP (Thermo Fisher, #MA1-21516). Blots were incubated in secondary antibody for
117 one hour at room temperature (anti-rabbit; Amersham, #NA934) (anti-mouse; Amersham, #NA931) and
118 visualized with Clarity Western ECL Substrate (Bio-Rad, #1705061) on a ChemiDoc Imaging System (Bio-
119 Rad).

120 **Drug Treatments**

121 Prior to all drug treatments, cells were deprived of estrogens by culturing them in phenol-red free
122 DMEM or RPMI supplemented with 10% charcoal stripped FBS (ssDMEM/ssRPMI; Cytiva, #SH30910.03,
123 stripped in-house), 1% Pen/Strep, 2 mM L-glutamine (Thermo Fisher, #25030-081), and 1 mM sodium
124 pyruvate (DMEM only) for three days. Cells were treated with vehicle (0.1% EtOH) or 10 nM 17β-estradiol
125 (E2; Millipore Sigma #E2257). The duration of each treatment is noted for each experiment.

126 **Knockdown of GRHL2 with siRNA**

127 For experiments involving GRHL2 knockdown, cells were reverse transfected with 25 nM of either
128 All Stars Negative control siRNA (siCtrl; QIAGEN, #1027280), siGRHL2 #1 (RNA-seq and qPCR validation
129 experiments) (Santa Cruz Biotechnology, #sc-77606), or siGRHL2 #2 (qPCR validation) (Dharmacon, #L-
130 014515-02-0050) using 2.5 ug/mL of Lipofectamine 2000 (Thermo Fisher Scientific, #11668019) in
131 Pen/Strep-free media.

132 **RNA Isolation and RT-qPCR**

133 RNA isolation was performed using the QIAGEN RNeasy Mini Kit (#74106) including treatment
134 with DNase (QIAGEN, #79254). Prior to qPCR, cDNA was generated using 1 µg of RNA and the iScript cDNA
135 Synthesis Kit (Bio-Rad, #1708891). qPCR was performed using iQ SYBR Green Supermix (Bio-Rad,
136 #1708884). Absolute quantification of RNA levels was performed by creating standard curves with
137 plasmids for *GRHL1* (Origene, #RC229312), *GRHL2* (Origene, #RG214498), and *GRHL3* (Origene,
138 #RC213012). The primers used were: *GRHL1*; Forward: 5'-ACAGCAAAAGAAACAGCATACCA-3' Reverse: 5'-
139 TTGCCATGGGGAAGGACAAT-3'. *GRHL2*; Forward: 5'-GCCACCAAATCTCTCCGTCA-3' Reverse: 5'-
140 CCACCATCACCACACTCCTG-3'. *GRHL3*; Forward: 5'-TGCAAGCGAGGAATCTTAGTCA-3' Reverse: 5'-
141 CTCGAGAGGCCTTACAGCTC-3'. Relative RNA levels were calculated using the ΔΔCt method. The primers
142 used were: *LYPD3*; Forward: 5'-TCACCTTGACGGCAGCTAAT-3' Reverse: 5'- GAACCCTGGGCCTGTTACTC-3'.
143 *EFEMP1*: Forward: 5'-TTATCATGGCGGCTTCCGTT-3' Reverse 5'-TGGGCAAACACATCGGTTCT-3'. *ARHGEF28*:

144 Forward: 5’-TGGAAAACTGCTACAGGTCGT-3’ Reverse 5’-ATGGCTTCTGATCAACGGCT-3’. *SCUBE2*: Forward:
145 5’-TTCACCGCTCGGAAGAGGG-3’ Reverse: 5’-TGGTTCTTGGCCAGCTCAAA-3’. *RPLP0* (housekeeping gene):
146 Forward: 5'-GACAATGGCAGCATCTACAAC-3' Reverse: 5'-GCAGACAGACACTGGCAAC-3'.

147 **RNA-seq**

148 MCF7 cells and T47D cells were cultured in 10 cm plates in ssDMEM and ssRPMI, respectively, for
149 two days. On day three, cells were transfected as described above at a density of 200,000 cell/well in 12-
150 well plates in Pen/Strep-free estrogen-deprived media. After 24 hours, media was changed to estrogen-
151 deprived media containing Pen/Strep and cells were treated with E2 or vehicle for 24 hours. RNA was then
152 isolated as described above. Samples for qPCR validation of RNA-seq were prepared using the same
153 process. Sequencing libraries were prepared using the Illumina TruSeq Stranded mRNA Library Prep kit
154 (Illumina, #20020595) and sequenced for 150bp paired-end reads on the NovaSeq6000 by the Next
155 Generation Sequencing department at the UW-Madison Biotechnology Center.

156 Quality control assessment of fastq files was performed using FASTQC (64). Adaptor trimming to
157 remove Illumina adaptors was performed using Cutadapt (65) through Trim Galore (66). Reads were
158 aligned to the hg38 genome with STAR (67). Aligned reads were assigned to genes using featureCounts
159 from the Subread package (68) and the hg38 NCBI RefSeq GTF (available at (69)) Differential gene
160 expression was performed using the DESeq2 package (70) with fold change shrinkage using ashr (71). PCA
161 plot was generated using DESeq2, heatmaps generated using pheatmap (72), and gene ontology was
162 performed using clusterProfiler (73).

163 **Migration Assays**

164 Migration assays were performed by seeding estrogen-deprived wild-type and CRISPR GRHL2
165 knockout cell pools obtained from Synthego (Menlo Park, CA) at a density of 700,000 cells/mL in Ibidi 4-
166 well dishes (Ibidi, #80406) simultaneously with vehicle or E2 treatment. 24 hours later, the 4 well insert

167 was removed to create a cell-free gap. The plates were imaged at 0 hours, 6 hours, and 24 hours, and the
168 gap was measured using the Wound Healing Size Tool plugin for imageJ (74).

169 **Cell Cycle Analysis**

170 Cells were deprived of estrogens for three days prior to adding treatments as described above for
171 24h, 48h, and 72h. Cell pellets were fixed in 100% ethanol and then resuspended in a staining solution
172 consisting of 100 ug/mL RNase A (Invitrogen, #12091021) and 50 ug/mL propidium iodide (Millipore
173 Sigma, #P4170). The dye intensity of 10,000 events was captured on a Thermo Fisher Attune NxT Flow
174 Cytometer. Analysis was performed using the ModFit software.

175 **CUT&RUN**

176 MCF7 cells were cultured in 10cm plates in ssDMEM for one day. On day two, cells were
177 transfected as described above at a density of 350,000 cell/well in 6-well plates. After 24 hours, the media
178 was changed to the appropriate media containing Pen/Strep. The following day, cells were removed from
179 the plates using brief trypsinization and assessed for viability using trypan blue (Gibco, #15250-061). $5x10^5$
180 viable cells were treated with vehicle or E2 for 30 min while rotating at 37ºC. Following treatment, samples
181 were processed for CUT&RUN using the CUTANA ChIC/CUT&RUN Kit (Epicypher, #14-1048; protocol from
182 user manual version 2.0). Antibodies used were ER (Epicypher, #13-2012), pS118-ER (Santa Cruz
183 Biotechnology, #sc-12915), GRHL2 (Millipore Sigma, #HPA004820), and IgG (Negative control; Epicypher,
184 #13-0042).

185 DNA concentrations were measured using the Qubit dsDNA HS assay kit (Thermo Fisher,
186 #Q33231). Library prep was performed using the NEBNext Ultra II DNA Library Prep Kit for Illumina (NEB,
187 #E7103) and NEBNext Multiplex Oligos for Illumina (NEB, #E6440), with changes made to the protocol to
188 improve the capture of smaller TF fragments: the inactivation temperature after end-repair was changed
189 to 50°C for 1 hour, the bead size-selection ratio in the adaptor cleanup step was increased to 1.75x, and
190 the bead size-selection ratio in the PCR cleanup step was increased to 1.2x (75, 76). Samples were

191 sequenced by paired-end 150bp sequencing on an Illumina NovaSeq 6000 by the Next Generation
192 Sequencing department at the UW-Madison Biotechnology Center.

193 Quality control assessment and adaptor trimming was performed as described in "RNA-seq".
194 Reads were aligned to the hg38 genome using Bowtie2 (77) using the --very-sensitive-local and --dovetail
195 flags. Aligned fragments were filtered for a maximum fragment length of 120bp using alignmentSieve
196 from Deeptools (78). Bam files from replicates were merged using Samtools merge. Peaks were called
197 with MACS2 (79) using IgG as a control and an FDR cutoff of 0.05. Peak overlaps were performed with
198 HOMER mergePeaks (80) with -d given. Heatmaps were plotted using Deeptools computeMatrix and
199 plotHeatmap.

200 **Generation of S118A ER mutation in MCF7 Cell Line**

201 Insertion of the S118A ER mutation in MCF7 cells was performed by following the Alt-R™ CRISPR-
202 Cas9 System Protocol (IDT; Coralville, IA, USA) for use with the Neon™ Transfection System (Thermo
203 Fisher, #MPK5000) with alterations specific for MCF7 cells. MCF7 cells were brought up at a low passage
204 (p2) as recommended by the electroporation protocol. Cells were grown in DMEM supplemented with
205 10% FBS and 1% Pen/Strep, split once, and then grown to confluency prior to cell counting and
206 electroporation. The crRNA:tracrRNA duplex was formed by resuspending the Alt-R™ CRISPR-Cas9 crRNA
207 (5' – TGCAGGAAAGGCGACAGCTG – 3') and Alt-R™ CRISPR-Cas9 tracrRNA (IDT, #1072532) in equimolar
208 concentrations in nuclease-free IDTE buffer (10 mM Tris, 0.1 mM EDTA, pH 7.5; IDT, #11-01-02-02) to a
209 final duplex concentration of 44 µM. The mixture was brought to 95°C for 5 min and allowed to cool to
210 room temperature. To form the RNP complex, Alt-R™ S.p. Cas9 Nuclease 3NLS (IDT, #1074181) was
211 resuspended in Resuspension Buffer R (Thermo Fisher) to a final concentration of 36 µM. For each
212 electroporation, equal volumes of the crRNA:tracrRNA duplex and RNP complex were combined and
213 incubated at room temp for 20 min. Prior to electroporation, MCF7 cells were collected, washed with
214 1xPBS, counted, and resuspended in Resuspension Buffer R to a concentration of 5 x 10^6 cells/mL. 8 µL of

215 the cell suspension was combined with the crRNA:tracrRNA:RNP complex, ssODN donor (5 –
216 CCCCCACTCAACAGCGTGTCTCCGAGCCCGCTGATGCTACTGCACCCGCCGCCGCAATTGGCGCCGTTCCTGC-
217 AGCCCCACGGCCAGCAGGTGCCCTACTACCTGGAGAACGAGCCCAGC – 3'), and Alt-R™ electroporation
218 enhancer (IDT, #1075915) for final concentrations of 1.8 µM crRNA:tracrRNA, 1.5 µM Cas9 RNP complex,
219 4 µM ssODN donor, and 1.8 µM electroporation enhancer. As a control, MCF7 cells with no
220 crRNA:tracrRNA were separately transfected keeping the same concentrations of the other components.
221 The final cell suspensions were electroporated using the Neon™ Transfection System with parameters set
222 for MCF7 cells (2 pulses, pulse voltage 1250v, pulse width 20ms). Cells were transferred to 12-well plates
223 with pre-warmed media without Pen/Strep and allowed to recover for 72 h.

224 **Screening of CRISPR-Cas9 clones**

225 After recovery, the cells were grown to confluency and cell populations were screened for
226 presence of the S118A mutation. DNA was isolated using the QIAGEN DNeasy Blood & Tissue Kit (QIAGEN,
227 #69504) and primers were generated to amplify around the region of interest (Forward: 5' –
228 GCCAACGCGCAGGTCTAC – 3'; Reverse: 5' – TCAAAGCGCCCCGTGTTTAT – 3'). Amplicons were subject to
229 digestion by SfoI (NEB, #R0606S) to test for the insertion of the S118A mutation. Populations positive for
230 SfoI digestion, indicating insertion of S118A mutation, underwent limiting dilution to identify single
231 colonies. Colonies were selected and expanded, followed by PCR screening and SfoI digestion as described
232 above. PCR amplicons from positive clones were additionally sequenced to confirm insertion of the S118A
233 mutation. Positive clones were further validated by induction of pS118-ER by E2 by Western blot analysis,
234 as described above.

235 **Chromatin Immunoprecipitation Sequencing (ChIP-seq)**

236 Cells were plated at a density of six million cells per 10cm plate with two plates per condition and
237 were deprived of estrogen for three days, followed by a 30-minute treatment with vehicle or E2. Samples
238 were prepared for ChIP as previously described (19) using a GRHL2 antibody (Millipore Sigma,

239 #HPA004820). DNA concentrations were measured using the Qubit dsDNA HS assay kit (Thermo Fisher,
240 #Q33231). Library prep was performed using the NEBNext Ultra II DNA Library Prep Kit for Illumina (NEB,
241 #E7103) and NEBNext Multiplex Oligos for Illumina (NEB, #E6440). Samples were sequenced by paired-
242 end 150bp sequencing on an Illumina NovaSeq 6000 by the Next Generation Sequencing department at
243 the UW-Madison Biotechnology Center.

244 Quality control assessment and adaptor trimming was performed as described in "RNA-seq".
245 Reads were aligned to the hg38 genome with Bowtie2 using --local and peaks were called with MACS2
246 using an FDR of 0.01. All peak file merging was performed using HOMER mergePeaks, -d given. For ChIP-
247 seq data from previous publications, data was downloaded using the SRA-Toolkit (81) from the following
248 accession numbers: pS118-ER/ER ChIP-seq (GSE117569) (19), GRHL2 ChIP-seq (GSE109820) (56), FOXA1
249 ChIP-seq (GSE59530) (82), p300 ChIP-seq (GSE60270) (83), H3K4me1/3 and H3K27ac ChIP-seq (GSE57436)
250 (84), and H3K27me3 ChIP-seq (GSE108787) (85). All data was trimmed and aligned using the previously
251 described methods with appropriate changes for single-end data. pS118-ER/ER and GRHL2 peaks were
252 called using the narrowpeak setting in MACS2 with FDR cutoffs of 0.01 and 0.05, respectively. Motif
253 analysis was performed using annotatePeaks.pl and findMotifsGenome.pl from HOMER.

254 **Statistical Methods**

255 The Wilcoxon rank sum test was used to analyze differences in RNA levels and percent gap closure.
256 A p-value less than 0.05 was considered significant.

257 **Data Availability**

258 The data reported in this paper have been deposited in the Gene Expression Omnibus (GEO)
259 database, www.ncbi.nlm.nih.gov/geo, under accession number GSE202622.

260 **RESULTS**

261 **GRHL2 expression is increased in ER-positive breast cancer compared to ER-negative**

262 The GRHL family is composed of three members, GRHL1, GRHL2, and GRHL3, all of which regulate
263 gene expression via the same DNA-binding motif (5'-AACCGGTT-3'). To characterize the GRHL family in
264 breast cancer, we first assessed the RNA expression of the GRHL family in normal breast tissue and breast
265 tumors using GEPIA2 (86). *GRHL2* expression was significantly increased in tumors than in normal breast,
266 whereas *GRHL1* and *GRHL3* showed no significant differences (Fig. 1A). These observations were further
267 supported by examination of TCGA datasets via cBioportal which showed that *GRHL2* was amplified in
268 10.8% of breast cancers while *GRHL1* and *GRHL3* were amplified in less than 1% of breast cancers (54, 87-
269 90).

270 An important consideration in treating breast cancer is the ER status of the tumor. We assessed
271 protein and RNA expression of the GRHL family in four ER-positive breast cancer cell lines (MCF7, T47D,
272 ZR-75-1, BT-474), and four ER-negative cell lines (BT-20, SK-BR-3, MDA-MB-468, MDA-MB-231). Each of
273 the GRHL family members is expressed in all evaluated cell lines, with the exception of MDA-MB-231
274 which lacks GRHL2 expression (Fig. 1B,C). *GRHL2* mRNA expression was significantly higher in ER-positive
275 than ER-negative cell lines, whereas *GRHL1* and *GRHL3* expression did not differ significantly between the
276 two categories (Fig. 1B). These results were further corroborated by a representative immunoblot of the
277 GRHL family in breast cancer cell lines (Fig. 1C). A previous study in primary breast tumors also found a
278 significant correlation between GRHL2 and ER expression (40). Given the proclivity for GRHL2 expression
279 in ER-positive breast cancer, we focused solely on GRHL2 for the remainder of our studies.

280 **pS118-ER/GRHL2 co-occupancy sites are found in enhancer regions**

281 In previous work from our group, we noted an enrichment of the GRHL2 motif near sites occupied
282 by ER phosphorylated at serine 118 (pS118-ER) (19). We asked whether there were differences in the
283 binding signals of pS118-ER/GRHL2 co-occupancy sites compared to those where each factor occupies

284 chromatin independently of the other. We took advantage of our own previously published pS118-ER and
285 ER ChIP-seq datasets (19) and a GRHL2 ChIP-seq performed in MCF7 cells treated with E2 for 30 and 45
286 minutes, respectively (56). The pS118-ER binding sites consist of a subset of sites within the total ER
287 binding sites. ER binding sites are defined as sites within the total ER binding set, excluding those that are
288 bound by pS118-ER. We identified 4,192 pS118-ER/GRHL2 co-occupancy sites and 4,028 ER/GRHL2 co-
289 occupancy sites which comprise 28% and 12% of total pS118-ER and total ER binding sites, respectively.
290 Of the binding sites occupied independently by each factor, we identified 33,797 ER sites (ER-only), 10,842
291 pS118-ER sites (pS118-ER-only), and 12,150 GRHL2 sites (GRHL2-only) (Fig. 2A). Of the co-occupancy
292 categories, GRHL2 binding was found prior to ligand treatment at 82.8% of the pS118-ER/GRHL2 co-
293 occupancy sites and 83.2% of the ER/GRHL2 co-occupancy sites, indicating GRHL2 can bind the majority
294 of these regions before E2-induced recruitment of ER (Fig. 2B). An example of a pS118-ER/GRHL2 co-
295 occupancy site is displayed in Fig. 2C. These results confirm GRHL2 is enriched at pS118-ER binding sites
296 relative to ER and indicate that GRHL2 and ER have both dependent and independent functions.

297 To further probe the relationship of ER, pS118-ER, and GRHL2 occupancy sites, we examined the
298 signal intensity in the five binding categories. Binding signal of pS118-ER is substantially higher than ER
299 sites, emphasizing the importance of this PTM in ER DNA binding (Fig. 2D, column 1, orange vs blue lines).
300 However, the binding signal of pS118-ER and ER at regions co-occupied by GRHL2 did not appear
301 noticeably different from regions where GRHL2 binding is absent (Fig. 2D, columns 1 and 2, solid vs dotted
302 lines). Similarly, the presence of pS118-ER or ER does not substantially affect the binding signal of GRHL2
303 (Fig. 2D, column 3, solid vs dotted lines). These data indicate ER/pS118-ER binding is not preferentially
304 stronger at GRHL2 binding sites and vice versa.

305 Previous studies showed GRHL2 can co-occupy chromatin with two factors that enhance ER
306 transcriptional activity: the pioneer factor FOXA1 (58, 63, 91) and p300, a histone acetyltransferase that
307 can deposit the enhancer histone mark H3K27ac (92, 93). We first asked whether the FOXA1 motif was

308 enriched at pS118-ER/GRHL2 co-occupancy sites. While the FOXA1 motif has comparable enrichment
309 across all categories with ER or pS118-ER binding, it is less prevalent at GRHL2-only binding sites (Fig. 3A),
310 suggesting that FOXA1 could be preferentially recruited to sites occupied by both ER and GRHL2 over
311 GRHL2 alone. Interestingly, the GRHL motif is the most prevalent motif at pS118-ER/GRHL2 and ER/GRHL2
312 co-occupancy sites while the ERE is most prevalent at pS118-ER-only and ER-only sites (Fig. 3A). Next, we
313 used previously published FOXA1 (82) and p300 (83) ChIP-seq studies performed in E2-treated MCF7 cells
314 (40 min and 1 hour treatments, respectively) to examine the presence of these two factors at pS118-
315 ER/GRHL2 co-occupancy sites (Fig. 3B). For both factors, the binding signal was strongest at pS118-
316 ER/GRHL2 co-occupancy sites followed by ER/GRHL2 co-occupancy sites and pS118-ER-only sites (Fig. 3B).
317 Analysis of the active enhancer marks H3K27ac and H3K4me1 ((84), 30 min treatment), the promoter
318 mark H3K4me3 ((84), 30 min treatment), and the repressive mark H3K27me3 ((85), 1 hour treatment)
319 further revealed an enrichment of H3K27ac and H3K4me1 at pS118-ER/GRHL2 co-occupancy sites and
320 ER/GRHL2 co-occupancy sites, relative to sites independently occupied by pS118-ER, ER, or GRHL2 alone
321 (Fig. 3B). The promotor mark H3K4me3 is enriched at GRHL2 only sites relative to co-occupancy sites with
322 pS118-ER and ER (Fig. 3B), which is consistent with the preferential localization of GRHL2 only sites in
323 promotor regions compared to any other binding category categories (9.5% vs 2.5-5.5%) (Fig. 3B,C). The
324 repressive H3K27me3 mark is weakest at pS118-ER/GRHL2 co-occupancy sites followed by ER/GRHL2 co-
325 occupancy sites (Fig. 3B). These data indicate pS118-ER/GRHL2 co-occupancy sites are enriched at active
326 enhancer regions.

327 **The loss of GRHL2 results in weaker pS118-ER DNA-binding**

328 Given the preference of pS118-ER/GRHL2 co-occupancy sites for enhancer regions compared to
329 either factor alone, we asked if GRHL2 is required for pS118-ER to bind to chromatin, and vice versa. First,
330 we assessed the requirement of GRHL2 for pS118-ER chromatin occupancy by performing CUT&RUN for
331 ER and pS118-ER in MCF7 cells depleted of GRHL2 using siRNA in the presence and absence of E2 (Fig. 4A).

332 There was no change in pS118-ER induction by E2 after depletion of GRHL2 (Fig. 4A). High-confidence
333 pS118-ER binding sites were identified by removing peaks that were detected in vehicle-treated cells and
334 peaks that were not detected by the total ER antibody. In mock-transfected E2-treated cells (siCtrl), we
335 identified 7,269 total ER and 2,860 pS118-ER binding sites. After the depletion of GRHL2, 4,171 ER sites
336 were lost (57%) and 1,089 ER sites were gained. 3,098 ER sites were maintained in both control and
337 GRHL2-depleted conditions (Fig. 4B,C). Both total ER and pS118-ER binding signals were substantially
338 decreased in GRHL2-depleted cells, including instances when ER binding was maintained in both control
339 and GRHL2-depleted conditions (Fig. 4C). Phosphorylation of S118 could be detected in control conditions
340 at 1,178 (28.2%) of the ER binding sites that were lost and 2,026 (65.4%) of ER binding sites that were
341 maintained in both control and GRHL2-depleted conditions (Fig. 4B,C). However, only 127 (11.7%) of new
342 ER binding sites identified in GRHL2-depleted conditions were phosphorylated at S118 (Fig. 4B,C). These
343 data indicate GRHL2 is required for robust pS118-ER DNA occupancy.

344 Conversely, to determine if the phosphorylation of S118 on ER is required for GRHL2 DNA-binding,
345 we performed ChIP-seq for GRHL2 in two independent MCF7 CRISPR knock-in cell lines in which the serine
346 at position 118 has been mutated to an alanine (S118A-ER), thereby preventing phosphorylation at this
347 site (Fig. 5A). In wild-type (WT) cells with intact pS118-ER, GRHL2 occupied 16,123 sites. In knock-in cell
348 lines with S118A-ER, GRHL2 occupied 14,682 sites in one clone (S118A #1), and 16,634 sites in the second
349 clone (S118A #2). The majority of binding sites (13,066) were shared among the three cell lines (Fig. 5B).
350 Further, GRHL2 DNA-binding signal in the two S118A mutants was comparable to the WT cells. Together,
351 these data indicate that pS118-ER is not reciprocally required for GRHL2 to bind DNA (Fig. 5C).

352 **GRHL2 and estrogen co-regulated genes are involved in cell migration**

353 After establishing that pS118-ER/GRHL2 co-occupancy sites bind preferentially in enhancer
354 regions and that GRHL2 is necessary for pS118-ER chromatin binding, we next investigated what genes
355 and biological processes these two factors co-regulate. To identify these genes, we performed RNA-seq

356 in triplicate in E2-treated MCF7 and T47D cells which had been depleted of GRHL2 using siRNA (Fig. 6A,
357 Supplemental Fig. 1A). E2 activation was confirmed by the induction of pS118-ER (12, 19) and
358 downregulation of total ER levels (94) (Fig. 6A, Supplemental Fig. 1A). As before, the loss of GRHL2 did not
359 affect E2-mediated pS118-ER induction (Fig. 6A, Supplemental Fig. 1A). Principle component analysis
360 (PCA) showed a large amount of variance between vehicle and E2 treatments in both cell lines, with a
361 larger variance observed in MCF7 cells (Fig. 6B, Supplemental Fig. 1B). There was a larger variance
362 between siCtrl and siGRHL2 in T47Ds than in MCF7s (Fig. 6B, Supplemental Fig. 1B). Differential expression
363 analysis was next performed using DESeq2 and the results were filtered for genes with an adjusted p-
364 value of less than 0.05 and a $\log_2$ fold change of greater than 1 or less than -1. Genes were defined as
365 primarily controlled by E2-activated ER (ER-only), primarily controlled by GRHL2 (GRHL2-only), or co-
366 regulated by both ER and GRHL2 (ER/GRHL2 co-regulated) (Fig. 6C, Supplemental Fig. 1C, Supplemental
367 Tables 1 and 2).

368 Examination of the ER/GRHL2 co-regulated genes revealed dual roles of GRHL2 in the regulation
369 of E2-mediated ER transcriptional activity. ER/GRHL2 co-regulated genes can be broken down into four
370 clusters (Fig. 6C,D, Supplemental Fig. 1C,D). When GRHL2 is lost, genes in clusters 1 and 4 show increased
371 downregulation and upregulation by estrogen, respectively. These data indicated that when GRHL2 is
372 present it opposes the regulatory action of ER on these genes. Genes in cluster 2 and 3 show decreased
373 downregulation and upregulation by ER when GRHL2 is lost. At these genes, when GRHL2 is present it
374 enhances ER transcriptional regulation. Using qRT-PCR and two independent siRNAs against *GRHL2,* we
375 validated these co-regulation patterns in a selection of genes: *LYPD3* (cluster 1), *EFEMP1* (cluster 2),
376 *ARHGEF28* (cluster 3), and *SCUBE2* (cluster 4) (Fig. 6E). Notably, *LYPD3* was previously identified as a
377 GRHL2 target gene in a tamoxifen resistant breast cancer cell line (63). These data demonstrate that
378 GRHL2 has pleiotropic effects on E2-induced pS118-ER transcriptional activity and can work as either a

379 transcriptional activator or repressor to influence the magnitude of estrogenic responses in a gene-
380 specific manner.

381 To determine which biological processes that ER/GRHL2 co-regulated genes may influence, we
382 performed gene ontology analysis using clusterProfiler. As expected, E2-only genes were primarily
383 associated with mitosis and cell cycle-related pathways (95) and GRHL2-only genes annotated to epithelial
384 terms such as "regulation of cell-cell adhesion" (24, 27, 31) and "wound healing" (96) (Supplemental Table
385 3). Gene ontology analysis of ER/GRHL2 co-regulated genes found four of the top ten most significant
386 pathways in MCF7s were related to cell migration and motility (Fig. 7A, Supplemental Table 3). To test the
387 effect of E2-activate ER and GRHL2 on migration, we took advantage of MCF7 cell pools which have
388 undergone CRISPR-mediated depletion of GRHL2 (GRHL2-KO) (Fig. 7B-D). Cells were treated with vehicle
389 or E2 for 24 hours prior to the creation of a cell-free gap. GRHL2-KO cells migrated across the cell-free gap
390 more quickly than wild type (WT) cells over the course of 24 hours, and migration was further enhanced
391 by the addition of E2. We determined the increase in migration was not a result of increased growth based
392 on cell cycle analysis which indicated the loss of GRHL2 did not impact E2-induced growth responses in
393 this time frame (Fig. 7E). These data indicate a co-regulatory role for GRHL2 and E2-induced pS118-ER in
394 regulating cell migration. In addition, these data demonstrate that GRHL2 is a critical blockade that inhibits
395 the migratory properties of MCF7 cells in the presence of activated ER.

396 **DISCUSSION**

397 Phosphorylation of S118 on the estrogen receptor is necessary for maximal ER-transcriptional
398 activity and chromatin-binding (12, 17, 19, 97). Our group identified a specific enrichment of the GRHL2
399 motif near pS118-ER occupancy sites suggesting an important role for GRHL2 in pS118-ER activity (19). In
400 this report we examined the co-dependency of GRHL2 and pS118-ER chromatin-occupancy and
401 transcriptional regulation of gene expression. We found that the loss of GRHL2 results in a global decrease
402 in pS118-ER chromatin-occupancy, demonstrating a critical role for GRHL2 in promoting maximal pS118-

403 ER recruitment to chromatin. GRHL2 can bind to chromatin prior to ligand treatment and pS118-ER/GRHL2
404 co-occupancy sites tend to be localized to active enhancer regions marked by H3K27ac and H3K4me1.
405 Transcriptionally, GRHL2 can both enhance and antagonize E2-induced pS118-ER transcriptional activity,
406 indicating a role for GRHL2 in tuning pS118-ER-mediated gene expression. These studies lead us to
407 propose a model in which GRHL2 primes chromatin prior to ligand treatment to facilitate the recruitment
408 of pS118-ER and then further fine tunes E2-mediated pS118-ER transcriptional activity through the
409 recruitment or repression of additional coregulators (Fig. 8). The full range of coregulators GRHL2 recruits
410 or interacts with are still unknown and may vary based on the genetic background of a given cell.

411 GRHL2 occupies sites destined to be co-bound by ER prior to E2-mediated ER activation, and
412 GRHL2 is necessary for robust pS118-ER DNA binding. In contrast, a S118A mutation in ER that prevents
413 phosphorylation failed to alter GRHL2 binding. These data suggest that GRHL2 primes enhancers for ER
414 binding events. Similar observations were made in studies of the highly conserved *Drosophila*
415 *melanogaster* homolog grainyhead (Grh) (98-101). These data have led to the hypothesis that the GRHL
416 family may function as pioneer factors, a specialized class of transcription factors that influence
417 transcriptional activity by promoting an open chromatin structure which promotes the recruitment of
418 other transcription factors (102, 103). Decreased Grh in the developing *D. melanogaster* and decreased
419 GRHL2 in epiblast-like cells resulted in a reduction of global chromatin accessibility (98, 99, 104). The same
420 was observed when all three mammalian GRHL family members were knocked down in MCF7 cells (98).
421 Another study using transgenic GFP reporters found Grh was bound to and promoted the accessibility of
422 various enhancer regions prior to their activation (98). Further, mutation of the Grh motif at a selection
423 of enhancers resulted in reduced chromatin accessibility (98). Interestingly, while the ERE is typically the
424 most highly enriched motif at pS118-ER occupancy sites (19), we instead discovered a high prevalence of
425 the GRHL motif at pS118-ER/GRHL2 co-occupancy sites. These data together suggest that the presence of

426 the GRHL motif may identify a select set of ER enhancers that require chromatin opening in order for
427 pS118-ER to bind DNA.

428 Previous studies have found GRHL2 can specifically associate with open and active enhancer
429 regions marked by H3K27ac and H3K4me1 (56, 104). In agreement, we observed an association of GRHL2
430 binding sites with H3K27ac and H3K4me1 in breast cancer cells, particularly when it co-occupied
431 chromatin with ER or pS118-ER. A previous study examining co-occupancy sites of GRHL2 and androgen
432 receptor (AR), another nuclear receptor, also found an enrichment of H3K27ac at co-occupancy sites
433 compared to either factor alone (35). These data suggest that other transcription factors and coregulators
434 are needed in addition to GRHL2 to fully engage active enhancers. We also found the strongest
435 enrichment of FOXA1 binding signal at pS118-ER/GRHL2 co-occupancy sites. FOXA1 frequently binds in
436 active enhancer regions marked by H3K4me1 (62) and is known to facilitate ER recruitment to chromatin
437 (105). GRHL2 has been shown to work in concert with FOXA1 to recruit the histone methyltransferase
438 MLL3 which in turn deposits H3K4me1 (58). GRHL2 can also directly interact with MLL3 via two amino
439 acids in the GRHL2 transactivation domain, suggesting it may directly recruit MLL3 (106). However,
440 regardless if MLL3 is present, GRHL2/FOXA1 co-occupancy sites also show stronger enrichment of
441 H3K4me1 than sites where either factor occupies chromatin individually (58). This suggests that other
442 coregulators may also contribute to H3K4me1 deposition at these sites. Overall, our data provide
443 additional evidence that the combination of GRHL2, FOXA1, and pS118-ER more faithfully mark active
444 enhancers than the individual factors.

445 Given the association of pS118-ER with upregulated genes (19) and the preference of GRHL2 and
446 pS118-ER for active enhancers, we were surprised to find in our transcriptomic analysis that GRHL2 can
447 both enhance and antagonize E2-mediated gene expression. This suggests that GRHL2 may interact with
448 other coregulators to modulate pS118-ER transcriptional function. As discussed above, these factors likely
449 include FOXA1 and MLL3, which are associated with marks of active enhancers. In this report we found

450 pS118-ER/GRHL2 co-occupancy sites display the strongest signal for the ER co-activator p300 (93, 107), a
451 histone acetyltransferase which can deposit the active enhancer mark H3K27ac (108). Although p300
452 could be responsible for the presence of H3K27ac at pS118-ER/GRHL2 co-occupancy sites, GRHL2 can
453 inhibit p300 activity via an interaction of a 13 amino acid segment of the GRHL2 DNA binding domain with
454 the C-terminal end of p300 (92). Based on this finding, it is possible that GRHL2 could inhibit p300/ER
455 transcriptional complexes leading to repression at select genes. Therefore, one explanation of how GRHL2
456 can either activate or repress pS118-ER gene transcription is via GRHL2 activity on other transcription
457 factors (FOXA1) or histone modifiers (MLL3, p300) that make up the pS118-ER transcriptional complex.
458 In addition to exploring the interplay between GRHL2 and pS118-ER in chromatin binding, we also
459 wanted to understand what biological processes are co-regulated by GRHL2 and E2-activated pS118-ER.
460 As expected, genes associated with cell cycle and epithelial cell integrity aligned with ER-only and GRHL-
461 only gene sets respectively, consistent with their well-described roles (24, 27, 31, 95, 96). Gene ontology
462 analysis of ER/GRHL2 co-regulated genes, however, showed a large proportion of co-regulated genes were
463 involved in migration. We subsequently found that the loss of GRHL2 can increase cell migration and this
464 effect is further enhanced by the addition of E2. A previous study in ER-negative cell lines also found
465 GRHL2 influences migration in a tumor suppressive manner (40), but this study is the first to show the co-
466 regulatory role of GRHL2 and ER in this phenotype. In the hormone-dependent ER-positive breast cancer
467 model tested here, GRHL2 serves as an important blockade that inhibits cell migration. An example of an
468 ER/GRHL2 co-regulated gene that was annotated to cell migration in the gene ontology analysis was
469 *SASH1*, a tumor suppressor that inhibits invasion and migration (109, 110). *SASH1* regulation is described
470 by cluster 1, in which E2 downregulates *SASH1* and GRHL2 depletion results in further downregulation of
471 *SASH1* expression. Regulation of *SASH1* may be an example of an instance where GRHL2 depletion results
472 in an expression threshold being crossed and factors like SASH1 can no longer enact their tumor
473 suppressive action, resulting in increased cell migration.

474 In summary, we have established a role for GRHL2 in facilitating the binding of pS118-ER to DNA
475 and have shown that sites co-occupied by GRHL2 and pS118-ER identify a set of enhancers marked by
476 H3K27ac and H3K4me1. We propose a model for the potential interactions among GRHL2, pS118-ER, and
477 other coregulators like p300 and FOXA1 to either complement or oppose pS118-ER transcriptional activity.
478 Finally, our data indicate that decreases in GRHL2 lead to increased cell migration that is further enhanced
479 by estrogen stimulation. These data identify dual activities of GRHL2 and its modulation of activated ER
480 and reveal a complexity to the interplay between GRHL2 and pS118-ER that impacts cancer phenotypes,
481 particularly migration.

482 **ACKNOWLEDGEMENTS**

483 We thank Kathryn Fox and the University of Wisconsin Carbone Comprehensive Cancer Center Flow
484 Cytometry Laboratory for their assistance with proliferation studies. We also thank Dr. David Lung for
485 his input into the manuscript. This work is supported by NIH grant R01 CA260140 to ETA.

486 **REFERENCES**

487 1. Green S, Walter P, Kumar V, Krust A, Bornert JM, Argos P, Chambon P. 1986. Human oestrogen
488 receptor cDNA: sequence, expression and homology to v-erb-A. Nature 320:134-9.
489 2. Sleightholm R, Neilsen BK, Elkhatib S, Flores L, Dukkipati S, Zhao R, Choudhury S, Gardner B,
490 Carmichael J, Smith L, Bennion N, Wahl A, Baine M. 2021. Percentage of Hormone Receptor
491 Positivity in Breast Cancer Provides Prognostic Value: A Single-Institute Study. J Clin Med Res
492 13:9-19.
493 3. Harvey JM, Clark GM, Osborne CK, Allred DC. 1999. Estrogen receptor status by
494 immunohistochemistry is superior to the ligand-binding assay for predicting response to
495 adjuvant endocrine therapy in breast cancer. J Clin Oncol 17:1474-81.
496 4. Tora L, White J, Brou C, Tasset D, Webster N, Scheer E, Chambon P. 1989. The human estrogen
497 receptor has two independent nonacidic transcriptional activation functions. Cell 59:477-87.
498 5. Webster NJ, Green S, Jin JR, Chambon P. 1988. The hormone-binding domains of the estrogen
499 and glucocorticoid receptors contain an inducible transcription activation function. Cell 54:199-
500 207.
501 6. Kumar V, Chambon P. 1988. The estrogen receptor binds tightly to its responsive element as a
502 ligand-induced homodimer. Cell 55:145-56.
503 7. Klein-Hitpass L, Ryffel GU, Heitlinger E, Cato AC. 1988. A 13 bp palindrome is a functional
504 estrogen responsive element and interacts specifically with estrogen receptor. Nucleic Acids Res
505 16:647-63.

506 8. Shiau AK, Barstad D, Loria PM, Cheng L, Kushner PJ, Agard DA, Greene GL. 1998. The structural
507 basis of estrogen receptor/coactivator recognition and the antagonism of this interaction by
508 tamoxifen. Cell 95:927-37.
509 9. Beato M, Sanchez-Pacheco A. 1996. Interaction of steroid hormone receptors with the
510 transcription initiation complex. Endocr Rev 17:587-609.
511 10. Heery DM, Kalkhoven E, Hoare S, Parker MG. 1997. A signature motif in transcriptional co-
512 activators mediates binding to nuclear receptors. Nature 387:733-6.
513 11. Le Romancer M, Poulard C, Cohen P, Sentis S, Renoir JM, Corbo L. 2011. Cracking the estrogen
514 receptor's posttranslational code in breast tumors. Endocr Rev 32:597-622.
515 12. Ali S, Metzger D, Bornert JM, Chambon P. 1993. Modulation of transcriptional activation by
516 ligand-dependent phosphorylation of the human oestrogen receptor A/B region. EMBO J
517 12:1153-60.
518 13. Bunone G, Briand PA, Miksicek RJ, Picard D. 1996. Activation of the unliganded estrogen
519 receptor by EGF involves the MAP kinase pathway and direct phosphorylation. EMBO J 15:2174-
520 83.
521 14. Sarwar N, Kim JS, Jiang J, Peston D, Sinnett HD, Madden P, Gee JM, Nicholson RI, Lykkesfeldt AE,
522 Shousha S, Coombes RC, Ali S. 2006. Phosphorylation of ERalpha at serine 118 in primary breast
523 cancer and in tamoxifen-resistant tumours is indicative of a complex role for ERalpha
524 phosphorylation in breast cancer progression. Endocr Relat Cancer 13:851-61.
525 15. Murphy L, Cherlet T, Adeyinka A, Niu Y, Snell L, Watson P. 2004. Phospho-serine-118 estrogen
526 receptor-alpha detection in human breast tumors in vivo. Clin Cancer Res 10:1354-9.
527 16. Cheng J, Zhang C, Shapiro DJ. 2007. A functional serine 118 phosphorylation site in estrogen
528 receptor-alpha is required for down-regulation of gene expression by 17beta-estradiol and 4-
529 hydroxytamoxifen. Endocrinology 148:4634-41.
530 17. Valley CC, Metivier R, Solodin NM, Fowler AM, Mashek MT, Hill L, Alarid ET. 2005. Differential
531 regulation of estrogen-inducible proteolysis and transcription by the estrogen receptor alpha N
532 terminus. Mol Cell Biol 25:5417-28.
533 18. Dutertre M, Smith CL. 2003. Ligand-independent interactions of p160/steroid receptor
534 coactivators and CREB-binding protein (CBP) with estrogen receptor-alpha: regulation by
535 phosphorylation sites in the A/B region depends on other receptor domains. Mol Endocrinol
536 17:1296-314.
537 19. Helzer KT, Szatkowski Ozers M, Meyer MB, Benkusky NA, Solodin N, Reese RM, Warren CL, Pike
538 JW, Alarid ET. 2019. The Phosphorylated Estrogen Receptor alpha (ER) Cistrome Identifies a
539 Subset of Active Enhancers Enriched for Direct ER-DNA Binding and the Transcription Factor
540 GRHL2. Mol Cell Biol 39.
541 20. Dynlacht BD, Attardi LD, Admon A, Freeman M, Tjian R. 1989. Functional analysis of NTF-1, a
542 developmentally regulated Drosophila transcription factor that binds neuronal cis elements.
543 Genes Dev 3:1677-88.
544 21. Wilanowski T, Tuckfield A, Cerruti L, O'Connell S, Saint R, Parekh V, Tao J, Cunningham JM, Jane
545 SM. 2002. A highly conserved novel family of mammalian developmental transcription factors
546 related to Drosophila grainyhead. Mech Dev 114:37-50.
547 22. Ming Q, Roske Y, Schuetz A, Walentin K, Ibraimi I, Schmidt-Ott KM, Heinemann U. 2018.
548 Structural basis of gene regulation by the Grainyhead/CP2 transcription factor family. Nucleic
549 Acids Res 46:2082-2095.
550 23. Ting SB, Caddy J, Hislop N, Wilanowski T, Auden A, Zhao LL, Ellis S, Kaur P, Uchida Y, Holleran
551 WM, Elias PM, Cunningham JM, Jane SM. 2005. A homolog of Drosophila grainy head is essential
552 for epidermal integrity in mice. Science 308:411-3.

553 24. Werth M, Walentin K, Aue A, Schonheit J, Wuebken A, Pode-Shakked N, Vilianovitch L, Erdmann
554 B, Dekel B, Bader M, Barasch J, Rosenbauer F, Luft FC, Schmidt-Ott KM. 2010. The transcription
555 factor grainyhead-like 2 regulates the molecular composition of the epithelial apical junctional
556 complex. Development 137:3835-45.
557 25. Ray HJ, Niswander LA. 2016. Grainyhead-like 2 downstream targets act to suppress epithelial-to-
558 mesenchymal transition during neural tube closure. Development 143:1192-204.
559 26. Rifat Y, Parekh V, Wilanowski T, Hislop NR, Auden A, Ting SB, Cunningham JM, Jane SM. 2010.
560 Regional neural tube closure defined by the Grainy head-like transcription factors. Dev Biol
561 345:237-45.
562 27. Pyrgaki C, Liu A, Niswander L. 2011. Grainyhead-like 2 regulates neural tube closure and
563 adhesion molecule expression during neural fold fusion. Dev Biol 353:38-49.
564 28. Walentin K, Hinze C, Werth M, Haase N, Varma S, Morell R, Aue A, Potschke E, Warburton D, Qiu
565 A, Barasch J, Purfurst B, Dieterich C, Popova E, Bader M, Dechend R, Staff AC, Yurtdas ZY, Kilic E,
566 Schmidt-Ott KM. 2015. A Grhl2-dependent gene network controls trophoblast branching
567 morphogenesis. Development 142:1125-36.
568 29. Narasimha M, Uv A, Krejci A, Brown NH, Bray SJ. 2008. Grainy head promotes expression of
569 septate junction proteins and influences epithelial morphogenesis. J Cell Sci 121:747-52.
570 30. Gao X, Bali AS, Randell SH, Hogan BL. 2015. GRHL2 coordinates regeneration of a polarized
571 mucociliary epithelium from basal stem cells. J Cell Biol 211:669-82.
572 31. Senga K, Mostov KE, Mitaka T, Miyajima A, Tanimizu N. 2012. Grainyhead-like 2 regulates
573 epithelial morphogenesis by establishing functional tight junctions through the organization of a
574 molecular network among claudin3, claudin4, and Rab25. Mol Biol Cell 23:2845-55.
575 32. Varma S, Mahavadi P, Sasikumar S, Cushing L, Hyland T, Rosser AE, Riccardi D, Lu J, Kalin TV,
576 Kalinichenko VV, Guenther A, Ramirez MI, Pardo A, Selman M, Warburton D. 2014. Grainyhead-
577 like 2 (GRHL2) distribution reveals novel pathophysiological differences between human
578 idiopathic pulmonary fibrosis and mouse models of pulmonary fibrosis. Am J Physiol Lung Cell
579 Mol Physiol 306:L405-19.
580 33. Adhikari N, Neupane S, Gwon GJ, Kim JY, An CH, Lee S, Sohn WJ, Lee Y, Kim JY. 2017. Grhl3
581 modulates epithelial structure formation of the circumvallate papilla during mouse
582 development. Histochem Cell Biol 147:5-16.
583 34. Mlacki M, Darido C, Jane SM, Wilanowski T. 2014. Loss of Grainy head-like 1 is associated with
584 disruption of the epidermal barrier and squamous cell carcinoma of the skin. PLoS One
585 9:e89247.
586 35. Paltoglou S, Das R, Townley SL, Hickey T, Tarulli G, Coutinho I, Fernandes RC, Hanson A, Denis I,
587 Carroll J, Dehm SM, Raj GV, Plymate S, Tilley WD, Selth LA. 2017. Novel androgen receptor co-
588 regulator GRHL2 exerts both oncogenic and anti-metastatic functions in prostate cancer. Cancer
589 Res doi:10.1158/0008-5472.CAN-16-1616.
590 36. Chung VY, Tan TZ, Tan M, Wong MK, Kuay KT, Yang Z, Ye J, Muller J, Koh CM, Guccione E, Thiery
591 JP, Huang RY. 2016. GRHL2-miR-200-ZEB1 maintains the epithelial status of ovarian cancer
592 through transcriptional regulation and histone modification. Sci Rep 6:19943.
593 37. Chen W, Yi JK, Shimane T, Mehrazarin S, Lin YL, Shin KH, Kim RH, Park NH, Kang MK. 2016.
594 Grainyhead-like 2 regulates epithelial plasticity and stemness in oral cancer cells. Carcinogenesis
595 37:500-10.
596 38. Pan X, Zhang R, Xie C, Gan M, Yao S, Yao Y, Jin J, Han T, Huang Y, Gong Y, Wang J, Yu B. 2017.
597 GRHL2 suppresses tumor metastasis via regulation of transcriptional activity of RhoG in non-
598 small cell lung cancer. Am J Transl Res 9:4217-4226.

599 39. Cieply B, Riley Pt, Pifer PM, Widmeyer J, Addison JB, Ivanov AV, Denvir J, Frisch SM. 2012.
600 Suppression of the epithelial-mesenchymal transition by Grainyhead-like-2. Cancer Res 72:2440-
601 53.
602 40. Werner S, Frey S, Riethdorf S, Schulze C, Alawi M, Kling L, Vafaizadeh V, Sauter G, Terracciano L,
603 Schumacher U, Pantel K, Assmann V. 2013. Dual roles of the transcription factor grainyhead-like
604 2 (GRHL2) in breast cancer. J Biol Chem 288:22993-3008.
605 41. Xiang J, Fu X, Ran W, Wang Z. 2017. Grhl2 reduces invasion and migration through inhibition of
606 TGFbeta-induced EMT in gastric cancer. Oncogenesis 6:e284.
607 42. Faddaoui A, Sheta R, Bachvarova M, Plante M, Gregoire J, Renaud MC, Sebastianelli A, Gobeil S,
608 Morin C, Ghani K, Bachvarov D. 2017. Suppression of the grainyhead transcription factor 2 gene
609 (GRHL2) inhibits the proliferation, migration, invasion and mediates cell cycle arrest of ovarian
610 cancer cells. Cell Cycle 16:693-706.
611 43. Yang X, Vasudevan P, Parekh V, Penev A, Cunningham JM. 2013. Bridging cancer biology with
612 the clinic: relative expression of a GRHL2-mediated gene-set pair predicts breast cancer
613 metastasis. PLoS One 8:e56195.
614 44. Nishino H, Takano S, Yoshitomi H, Suzuki K, Kagawa S, Shimazaki R, Shimizu H, Furukawa K,
615 Miyazaki M, Ohtsuka M. 2017. Grainyhead-like 2 (GRHL2) regulates epithelial plasticity in
616 pancreatic cancer progression. Cancer Med 6:2686-2696.
617 45. Kang X, Chen W, Kim RH, Kang MK, Park NH. 2009. Regulation of the hTERT promoter activity by
618 MSH2, the hnRNPs K and D, and GRHL2 in human oral squamous cell carcinoma cells. Oncogene
619 28:565-74.
620 46. Tanaka Y, Kanai F, Tada M, Tateishi R, Sanada M, Nannya Y, Ohta M, Asaoka Y, Seto M, Shiina S,
621 Yoshida H, Kawabe T, Yokosuka O, Ogawa S, Omata M. 2008. Gain of GRHL2 is associated with
622 early recurrence of hepatocellular carcinoma. J Hepatol 49:746-57.
623 47. Quan Y, Jin R, Huang A, Zhao H, Feng B, Zang L, Zheng M. 2014. Downregulation of GRHL2
624 inhibits the proliferation of colorectal cancer cells by targeting ZEB1. Cancer Biol Ther 15:878-87.
625 48. Quan Y, Xu M, Cui P, Ye M, Zhuang B, Min Z. 2015. [Expression and clinical significance of GRHL2
626 in colorectal cancer]. Zhonghua Zhong Liu Za Zhi 37:764-8.
627 49. Pawlak M, Kikulska A, Wrzesinski T, Rausch T, Kwias Z, Wilczynski B, Benes V, Wesoly J,
628 Wilanowski T. 2017. Potential Protective Role of Grainyhead-like Genes in the Development of
629 Clear Cell Renal Cell Carcinoma. Mol Carcinog doi:10.1002/mc.22682.
630 50. Butz H, Szabo PM, Nofech-Mozes R, Rotondo F, Kovacs K, Mirham L, Girgis H, Boles D, Patocs A,
631 Yousef GM. 2014. Integrative bioinformatics analysis reveals new prognostic biomarkers of clear
632 cell renal cell carcinoma. Clin Chem 60:1314-26.
633 51. Xiang J, Fu X, Ran W, Chen X, Hang Z, Mao H, Wang Z. 2013. Expression and role of grainyhead-
634 like 2 in gastric cancer. Med Oncol 30:714.
635 52. Torres-Reyes LA, Alvarado-Ruiz L, Pina-Sanchez P, Martinez-Silva MG, Ramos-Solano M, Olimon-
636 Andalon V, Ortiz-Lazareno PC, Hernandez-Flores G, Bravo-Cuellar A, Aguilar-Lemarroy A, Jave-
637 Suarez LF. 2014. Expression of transcription factor grainyhead-like 2 is diminished in cervical
638 cancer. Int J Clin Exp Pathol 7:7409-18.
639 53. Xiang X, Deng Z, Zhuang X, Ju S, Mu J, Jiang H, Zhang L, Yan J, Miller D, Zhang HG. 2013.
640 Correction: grhl2 determines the epithelial phenotype of breast cancers and promotes tumor
641 progression. PLoS One 8.
642 54. Reese RM, Harrison MM, Alarid ET. 2019. Grainyhead-like Protein 2: The Emerging Role in
643 Hormone-Dependent Cancers and Epigenetics. Endocrinology 160:1275-1288.
644 55. Mohammed H, D'Santos C, Serandour AA, Ali HR, Brown GD, Atkins A, Rueda OM, Holmes KA,
645 Theodorou V, Robinson JL, Zwart W, Saadi A, Ross-Innes CS, Chin SF, Menon S, Stingl J, Palmieri

646 C, Caldas C, Carroll JS. 2013. Endogenous purification reveals GREB1 as a key estrogen receptor
647 regulatory factor. Cell Rep 3:342-9.
648 56. Holding AN, Giorgi FM, Donnelly A, Cullen AE, Nagarajan S, Selth LA, Markowetz F. 2019.
649 VULCAN integrates ChIP-seq with patient-derived co-expression networks to identify GRHL2 as a
650 key co-regulator of ERa at enhancers in breast cancer. Genome Biol 20:91.
651 57. Chi D, Singhal H, Li L, Xiao T, Liu W, Pun M, Jeselsohn R, He H, Lim E, Vadhi R, Rao P, Long H,
652 Garber J, Brown M. 2019. Estrogen receptor signaling is reprogrammed during breast
653 tumorigenesis. Proc Natl Acad Sci U S A 116:11437-11443.
654 58. Jozwik KM, Chernukhin I, Serandour AA, Nagarajan S, Carroll JS. 2016. FOXA1 Directs H3K4
655 Monomethylation at Enhancers via Recruitment of the Methyltransferase MLL3. Cell Rep
656 17:2715-2723.
657 59. Heintzman ND, Stuart RK, Hon G, Fu Y, Ching CW, Hawkins RD, Barrera LO, Van Calcar S, Qu C,
658 Ching KA, Wang W, Weng Z, Green RD, Crawford GE, Ren B. 2007. Distinct and predictive
659 chromatin signatures of transcriptional promoters and enhancers in the human genome. Nat
660 Genet 39:311-8.
661 60. Cirillo LA, Lin FR, Cuesta I, Friedman D, Jarnik M, Zaret KS. 2002. Opening of compacted
662 chromatin by early developmental transcription factors HNF3 (FoxA) and GATA-4. Mol Cell
663 9:279-89.
664 61. Cirillo LA, McPherson CE, Bossard P, Stevens K, Cherian S, Shim EY, Clark KL, Burley SK, Zaret KS.
665 1998. Binding of the winged-helix transcription factor HNF3 to a linker histone site on the
666 nucleosome. EMBO J 17:244-54.
667 62. Lupien M, Eeckhoute J, Meyer CA, Wang Q, Zhang Y, Li W, Carroll JS, Liu XS, Brown M. 2008.
668 FoxA1 translates epigenetic signatures into enhancer-driven lineage-specific transcription. Cell
669 132:958-70.
670 63. Cocce KJ, Jasper JS, Desautels TK, Everett L, Wardell S, Westerling T, Baldi R, Wright TM, Tavares
671 K, Yllanes A, Bae Y, Blitzer JT, Logsdon C, Rakiec DP, Ruddy DA, Jiang T, Broadwater G, Hyslop T,
672 Hall A, Laine M, Phung L, Greene GL, Martin LA, Pancholi S, Dowsett M, Detre S, Marks JR,
673 Crawford GE, Brown M, Norris JD, Chang CY, McDonnell DP. 2019. The Lineage Determining
674 Factor GRHL2 Collaborates with FOXA1 to Establish a Targetable Pathway in Endocrine Therapy-
675 Resistant Breast Cancer. Cell Rep 29:889-903 e10.
676 64. FASTQC. https://www.bioinformatics.babraham.ac.uk/projects/fastqc/. Accessed May 7th,
677 2020.
678 65. Martin M. 2011. Cutadapt removes adapter sequences from high-throughput sequencing reads.
679 EMBnetjournal 17:10-12.
680 66. TrimGalore. https://github.com/FelixKrueger/TrimGalore. Accessed May 7th, 2020.
681 67. Dobin A, Davis CA, Schlesinger F, Drenkow J, Zaleski C, Jha S, Batut P, Chaisson M, Gingeras TR.
682 2013. STAR: ultrafast universal RNA-seq aligner. Bioinformatics 29:15-21.
683 68. Liao Y, Smyth GK, Shi W. 2014. featureCounts: an efficient general purpose program for
684 assigning sequence reads to genomic features. Bioinformatics 30:923-30.
685 69. NCBI. hg38 RefSeq GTF.
686 http://ftp.ensembl.org/pub/current_gtf/homo_sapiens/Homo_sapiens.GRCh38.104.gtf.gz.
687 Accessed November 10th, 2020.
688 70. Love MI, Huber W, Anders S. 2014. Moderated estimation of fold change and dispersion for
689 RNA-seq data with DESeq2. Genome Biol 15:550.
690 71. Stephens M. 2017. False discovery rates: a new deal. Biostatistics 18:275-294.
691 72. pheatmap. https://github.com/raivokolde/pheatmap. Accessed December 5th, 2020.

692 73. Wu T, Hu E, Xu S, Chen M, Guo P, Dai Z, Feng T, Zhou L, Tang W, Zhan L, Fu X, Liu S, Bo X, Yu G.
693 2021. clusterProfiler 4.0: A universal enrichment tool for interpreting omics data. Innovation (N
694 Y) 2:100141.
695 74. Suarez-Arnedo A, Torres Figueroa F, Clavijo C, Arbelaez P, Cruz JC, Munoz-Camargo C. 2020. An
696 image J plugin for the high throughput image analysis of in vitro scratch wound healing assays.
697 PLoS One 15:e0232565.
698 75. Liu N, Hargreaves VV, Zhu Q, Kurland JV, Hong J, Kim W, Sher F, Macias-Trevino C, Rogers JM,
699 Kurita R, Nakamura Y, Yuan GC, Bauer DE, Xu J, Bulyk ML, Orkin SH. 2018. Direct Promoter
700 Repression by BCL11A Controls the Fetal to Adult Hemoglobin Switch. Cell 173:430-442 e17.
701 76. Zhu Q, Liu N, Orkin SH, Yuan GC. 2019. CUT&RUNTools: a flexible pipeline for CUT&RUN
702 processing and footprint analysis. Genome Biol 20:192.
703 77. Langmead B, Salzberg SL. 2012. Fast gapped-read alignment with Bowtie 2. Nat Methods 9:357-
704 9.
705 78. Ramirez F, Ryan DP, Gruning B, Bhardwaj V, Kilpert F, Richter AS, Heyne S, Dundar F, Manke T.
706 2016. deepTools2: a next generation web server for deep-sequencing data analysis. Nucleic
707 Acids Res 44:W160-5.
708 79. Zhang Y, Liu T, Meyer CA, Eeckhoute J, Johnson DS, Bernstein BE, Nusbaum C, Myers RM, Brown
709 M, Li W, Liu XS. 2008. Model-based analysis of ChIP-Seq (MACS). Genome Biol 9:R137.
710 80. Heinz S, Benner C, Spann N, Bertolino E, Lin YC, Laslo P, Cheng JX, Murre C, Singh H, Glass CK.
711 2010. Simple combinations of lineage-determining transcription factors prime cis-regulatory
712 elements required for macrophage and B cell identities. Mol Cell 38:576-89.
713 81. SRA-Toolkit. https://trace.ncbi.nlm.nih.gov/Traces/sra/sra.cgi?view=software. Accessed April
714 21st, 2020.
715 82. Franco HL, Nagari A, Kraus WL. 2015. TNFalpha signaling exposes latent estrogen receptor
716 binding sites to alter the breast cancer cell transcriptome. Mol Cell 58:21-34.
717 83. Liu Z, Merkurjev D, Yang F, Li W, Oh S, Friedman MJ, Song X, Zhang F, Ma Q, Ohgi KA, Krones A,
718 Rosenfeld MG. 2014. Enhancer activation requires trans-recruitment of a mega transcription
719 factor complex. Cell 159:358-73.
720 84. Brunelle M, Nordell Markovits A, Rodrigue S, Lupien M, Jacques PE, Gevry N. 2015. The histone
721 variant H2A.Z is an important regulator of enhancer activity. Nucleic Acids Res 43:9742-56.
722 85. Zhou Y, Gerrard DL, Wang J, Li T, Yang Y, Fritz AJ, Rajendran M, Fu X, Stein G, Schiff R, Lin S,
723 Frietze S, Jin VX. 2019. Temporal dynamic reorganization of 3D chromatin architecture in
724 hormone-induced breast cancer and endocrine resistance. Nat Commun 10:1522.
725 86. Tang Z, Li C, Kang B, Gao G, Li C, Zhang Z. 2017. GEPIA: a web server for cancer and normal gene
726 expression profiling and interactive analyses. Nucleic Acids Res 45:W98-W102.
727 87. Kotarba G, Taracha-Wisniewska A, Wilanowski T. 2020. Grainyhead-like transcription factors in
728 cancer - Focus on recent developments. Exp Biol Med (Maywood) 245:402-410.
729 88. Hoadley KA, Yau C, Hinoue T, Wolf DM, Lazar AJ, Drill E, Shen R, Taylor AM, Cherniack AD,
730 Thorsson V, Akbani R, Bowlby R, Wong CK, Wiznerowicz M, Sanchez-Vega F, Robertson AG,
731 Schneider BG, Lawrence MS, Noushmehr H, Malta TM, Cancer Genome Atlas N, Stuart JM, Benz
732 CC, Laird PW. 2018. Cell-of-Origin Patterns Dominate the Molecular Classification of 10,000
733 Tumors from 33 Types of Cancer. Cell 173:291-304 e6.
734 89. Cerami E, Gao J, Dogrusoz U, Gross BE, Sumer SO, Aksoy BA, Jacobsen A, Byrne CJ, Heuer ML,
735 Larsson E, Antipin Y, Reva B, Goldberg AP, Sander C, Schultz N. 2012. The cBio cancer genomics
736 portal: an open platform for exploring multidimensional cancer genomics data. Cancer Discov
737 2:401-4.

738 90. Gao J, Aksoy BA, Dogrusoz U, Dresdner G, Gross B, Sumer SO, Sun Y, Jacobsen A, Sinha R,
739 Larsson E, Cerami E, Sander C, Schultz N. 2013. Integrative analysis of complex cancer genomics
740 and clinical profiles using the cBioPortal. Sci Signal 6:pl1.
741 91. Hurtado A, Holmes KA, Ross-Innes CS, Schmidt D, Carroll JS. 2011. FOXA1 is a key determinant of
742 estrogen receptor function and endocrine response. Nat Genet 43:27-33.
743 92. Pifer PM, Farris JC, Thomas AL, Stoilov P, Denvir J, Smith DM, Frisch SM. 2016. Grainyhead-like 2
744 inhibits the coactivator p300, suppressing tubulogenesis and the epithelial-mesenchymal
745 transition. Mol Biol Cell 27:2479-92.
746 93. Hanstein B, Eckner R, DiRenzo J, Halachmi S, Liu H, Searcy B, Kurokawa R, Brown M. 1996. p300
747 is a component of an estrogen receptor coactivator complex. Proc Natl Acad Sci U S A 93:11540-
748 5.
749 94. Alarid ET, Bakopoulos N, Solodin N. 1999. Proteasome-mediated proteolysis of estrogen
750 receptor: a novel component in autologous down-regulation. Mol Endocrinol 13:1522-34.
751 95. Prall OW, Rogan EM, Sutherland RL. 1998. Estrogen regulation of cell cycle progression in breast
752 cancer cells. J Steroid Biochem Mol Biol 65:169-74.
753 96. Boglev Y, Wilanowski T, Caddy J, Parekh V, Auden A, Darido C, Hislop NR, Cangkrama M, Ting SB,
754 Jane SM. 2011. The unique and cooperative roles of the Grainy head-like transcription factors in
755 epidermal development reflect unexpected target gene specificity. Dev Biol 349:512-22.
756 97. Kato S, Endoh H, Masuhiro Y, Kitamoto T, Uchiyama S, Sasaki H, Masushige S, Gotoh Y, Nishida E,
757 Kawashima H, Metzger D, Chambon P. 1995. Activation of the estrogen receptor through
758 phosphorylation by mitogen-activated protein kinase. Science 270:1491-4.
759 98. Jacobs J, Atkins M, Davie K, Imrichova H, Romanelli L, Christiaens V, Hulselmans G, Potier D,
760 Wouters J, Taskiran, II, Paciello G, Gonzalez-Blas CB, Koldere D, Aibar S, Halder G, Aerts S. 2018.
761 The transcription factor Grainy head primes epithelial enhancers for spatiotemporal activation
762 by displacing nucleosomes. Nat Genet 50:1011-1020.
763 99. Nevil M, Bondra ER, Schulz KN, Kaplan T, Harrison MM. 2017. Stable Binding of the Conserved
764 Transcription Factor Grainy Head to its Target Genes Throughout Drosophila melanogaster
765 Development. Genetics 205:605-620.
766 100. Nevil M, Gibson TJ, Bartolutti C, Iyengar A, Harrison MM. 2020. Establishment of chromatin
767 accessibility by the conserved transcription factor Grainy head is developmentally regulated.
768 Development 147.
769 101. Potier D, Davie K, Hulselmans G, Naval Sanchez M, Haagen L, Huynh-Thu VA, Koldere D, Celik A,
770 Geurts P, Christiaens V, Aerts S. 2014. Mapping gene regulatory networks in Drosophila eye
771 development by large-scale transcriptome perturbations and motif inference. Cell Rep 9:2290-
772 303.
773 102. Magnani L, Eeckhoute J, Lupien M. 2011. Pioneer factors: directing transcriptional regulators
774 within the chromatin environment. Trends Genet 27:465-74.
775 103. Zaret KS, Carroll JS. 2011. Pioneer transcription factors: establishing competence for gene
776 expression. Genes Dev 25:2227-41.
777 104. Chen AF, Liu AJ, Krishnakumar R, Freimer JW, DeVeale B, Blelloch R. 2018. GRHL2-Dependent
778 Enhancer Switching Maintains a Pluripotent Stem Cell Transcriptional Subnetwork after Exit
779 from Naive Pluripotency. Cell Stem Cell doi:10.1016/j.stem.2018.06.005.
780 105. Carroll JS, Liu XS, Brodsky AS, Li W, Meyer CA, Szary AJ, Eeckhoute J, Shao W, Hestermann EV,
781 Geistlinger TR, Fox EA, Silver PA, Brown M. 2005. Chromosome-wide mapping of estrogen
782 receptor binding reveals long-range regulation requiring the forkhead protein FoxA1. Cell
783 122:33-43.

784 106. MacFawn I, Wilson H, Selth LA, Leighton I, Serebriiskii I, Bleackley RC, Elzamzamy O, Farris J, Pifer
785 PM, Richer J, Frisch SM. 2019. Grainyhead-like-2 confers NK-sensitivity through interactions with
786 epigenetic modifiers. Mol Immunol 105:137-149.
787 107. Kraus WL, Kadonaga JT. 1998. p300 and estrogen receptor cooperatively activate transcription
788 via differential enhancement of initiation and reinitiation. Genes Dev 12:331-42.
789 108. Martire S, Nguyen J, Sundaresan A, Banaszynski LA. 2020. Differential contribution of p300 and
790 CBP to regulatory element acetylation in mESCs. BMC Mol Cell Biol 21:55.
791 109. Martini M, Gnann A, Scheikl D, Holzmann B, Janssen KP. 2011. The candidate tumor suppressor
792 SASH1 interacts with the actin cytoskeleton and stimulates cell-matrix adhesion. Int J Biochem
793 Cell Biol 43:1630-40.
794 110. Jiang K, Liu P, Xu H, Liang D, Fang K, Du S, Cheng W, Ye L, Liu T, Zhang X, Gong P, Shao S, Wang Y,
795 Meng S. 2020. SASH1 suppresses triple-negative breast cancer cell invasion through YAP-
796 ARHGAP42-actin axis. Oncogene 39:5015-5030.

797

798 **FIGURE LEGENDS**

799 **Figure 1: GRHL2 expression is higher in ER-positive vs ER-negative breast cancer.** A) mRNA expression of
800 the *GRHL* family in normal and tumor breast tissue obtained from GEPIA2. A * indicates a p-value < 0.05.
801 B) Absolute quantification of *GRHL* mRNA and in a panel of ER-positive and ER-negative breast cancer cell
802 lines. Error bars represent mean ± standard error. C) Representative Western blot of GRHL protein levels
803 in the same cell panel. β-actin is used as a loading control.

804 **Figure 2: Identification of pS118-ER/GRHL2 co-occupancy sites.** A) Venn diagram showing the overlap of
805 MCF7 E2-treated total ER, pS118-ER, and GRHL2 ChIP-seq datasets. pS118-ER binding sites are a subset of
806 total ER bindings sites. ER sites are defined as those that do not overlap with the pS118-ER dataset. Five
807 binding categories were established: pS118-ER/GRHL2 co-occupancy (4,192 sites), ER/GRHL2 co-
808 occupancy (4,028 sites), pS118-ER-only (10,842 sites), ER-only (33,797 sites), and GRHL2-only (12,150
809 sites). B) Venn diagrams showing the overlap of pS118-ER/GRHL2 co-occupancy sites and ER/GRHL2 co-
810 occupancy sites with GRHL2 peaks detected in vehicle conditions. C) Representative genome browser
811 track of a pS118-ER/GRHL2 co-occupancy site. D) Heatmaps showing binding signal of ER, pS118-ER, and
812 GRHL2 at each of the five binding categories. Data were obtained from previously published ChIP-seq
813 datasets (56).

814 **Figure 3: pS118-ER/GRHL2 co-occupancy sites are located at enhancers.** A) Motif analysis of the GRHL,
815 ERE, and FOXA1 motifs at co-occupancy sites. The first column shows enrichment of the indicated motif
816 (ERE in blue, GRHL in green, FOXA1 in purple) relative to the peak center. The second column shows the
817 percent of sites with each of the motifs. C) Heatmaps showing binding signal of FOXA1 and p300 and
818 metaplots showing the signal of the histone modifications H3K4me1, H3K4me3, H3K27ac, and H3K27me3
819 at each of the previously established binding categories. Data were obtained from previously published
820 ChIP-seq datasets (82-85). C) Genome location annotation of the five binding categories. Sites were
821 annotated to introns, intergenic regions, promoters, exons, or other. Promoters were defined as -1kb to
822 +100bp from the transcription start site.

823 **Figure 4: The loss of GRHL2 causes a reduction in ER and pS118-ER chromatin binding.** A) Representative
824 western blot of MCF7 samples used in CUT&RUN experiments. Cells were transfected with siCtrl or
825 siGRHL2 and treated for 30 minutes with vehicle or 10 nM E2. β-actin is used as a loading control. B) Venn
826 diagram and upset plot indicating the overlap of ER and pS118-ER CUT&RUN peaks in E2-treated, siCtrl-
827 or siGRHL2-transfected cells. C) Heatmaps showing CUT&RUN signal for ER, pS118-ER, and GRHL2 at lost
828 ER sites (purple), maintained ER siCtrl/siGRHL2 sites (purple and green dashed), and gained ER sites
829 (green). The percent of ER sites detected by the pS118-ER antibody are indicated in region labels.

830 **Figure 5: Loss of pS118-ER does not affect GRHL2 chromatin binding.** A) Representative western blot of
831 WT and S118A mutant MCF7 cells used for ChIP-seq. Cells were treated for 30min with vehicle or 10 nM
832 E2. TBP is used as a loading control. B) Venn diagrams showing the overlap of E2 GRHL2 binding sites
833 between WT cells and two S118A mutant clones. C) Heatmaps showing GRHL2 binding signal at collective
834 GRHL2 binding sites across all three cell lines.

835 **Figure 6: GRHL2 can enhance and antagonize E2-mediated ER transcriptional activity.** A) Representative
836 Western blot of MCF7 samples used in RNA-seq. Cells were transfected with siCtrl or siGRHL2 and treated

837 for 24 hours with vehicle or 10 nM E2. β-actin is used as a loading control. B) PCA plot of MCF7 RNA-seq
838 data displaying differences between siCtrl (purple), siGRHL2 (green), vehicle treatment (circles), and E2
839 treatment (triangles). C) Heatmap showing the expression of ER/GRHL2 co-regulated genes, ER-only
840 regulated genes, and GRHL2-only regulated genes. D) Gene expression profiles of ER/GRHL2 co-regulated
841 gene clusters. Error bars represent mean ± standard error. E) qPCR validation of selected genes from each
842 of the ER/GRHL2 co-regulated gene clusters using two different siRNAs against *GRHL2*. All values are
843 relative to siCtrl Veh. Error bars represent mean ± standard error.

844 **Figure 7: GRHL2 and E2 co-regulate migration.** A) Gene ontology analysis for biological processes
845 performed with clusterProfiler on ER/GRHL2 co-regulated genes. Terms related to cell migration, motility,
846 and locomotion are highlighted in red. The size of the dots represents the number of genes annotated to
847 a given term, and color represents the adjusted p-value with red being the most significant. B) Brightfield
848 images of WT and GRHL2-KO cell migration across a cell-free gap over the course of 24 hours. C)
849 Representative Western blot showing the loss of GRHL2 in pooled CRISPR GRHL2-KO cells. D)
850 Quantification of the percent gap closure over 6 hours and 24 hours. Error bars represent mean ± standard
851 error and * indicates a p-value < 0.05. E) Flow cytometry analysis showing the percent of cells in each of
852 the cell cycle stages (S, G2, G1). WT and GRHL2-KO cells were treated with vehicle or 10 nM E2 over 24h,
853 48h, and 72h. Error bars represent mean ± standard error.

854 **Figure 8: Model of GRHL2 function in facilitating pS118-ER binding and transcriptional activity.** GRHL2
855 binds to the GRHL motif in enhancers prior to ligand treatment. Upon exposure to E2, GRHL2 can either
856 promote gene transcription by facilitating the recruitment of coregulators like MLL3, or repress gene
857 transcription by repressing coregulators, like p300.

858 **Supplemental Figure 1: Similar patterns of GRHL2 regulation of E2-mediated ER transcriptional activity**
859 **are observed in T47D cells.** A) Representative Western blot of T47D samples used in RNA-seq. Cells were

860 transfected with siCtrl or siGRHL2 and treated for 24 hours with vehicle or 10 nM E2. β-actin is used as a
861 loading control. B) PCA plot of T47D RNA-seq data displaying differences between siCtrl (purple), siGRHL2
862 (green), vehicle treatment (circles), and E2 treatment (triangles). C) Heatmap showing the expression of
863 ER/GRHL2 co-regulated genes, E2-only regulated genes, and GRHL2-only regulated genes. D) Gene
864 expression profiles of ER/GRHL2 co-regulated gene clusters. Error bars represent mean ± standard error.

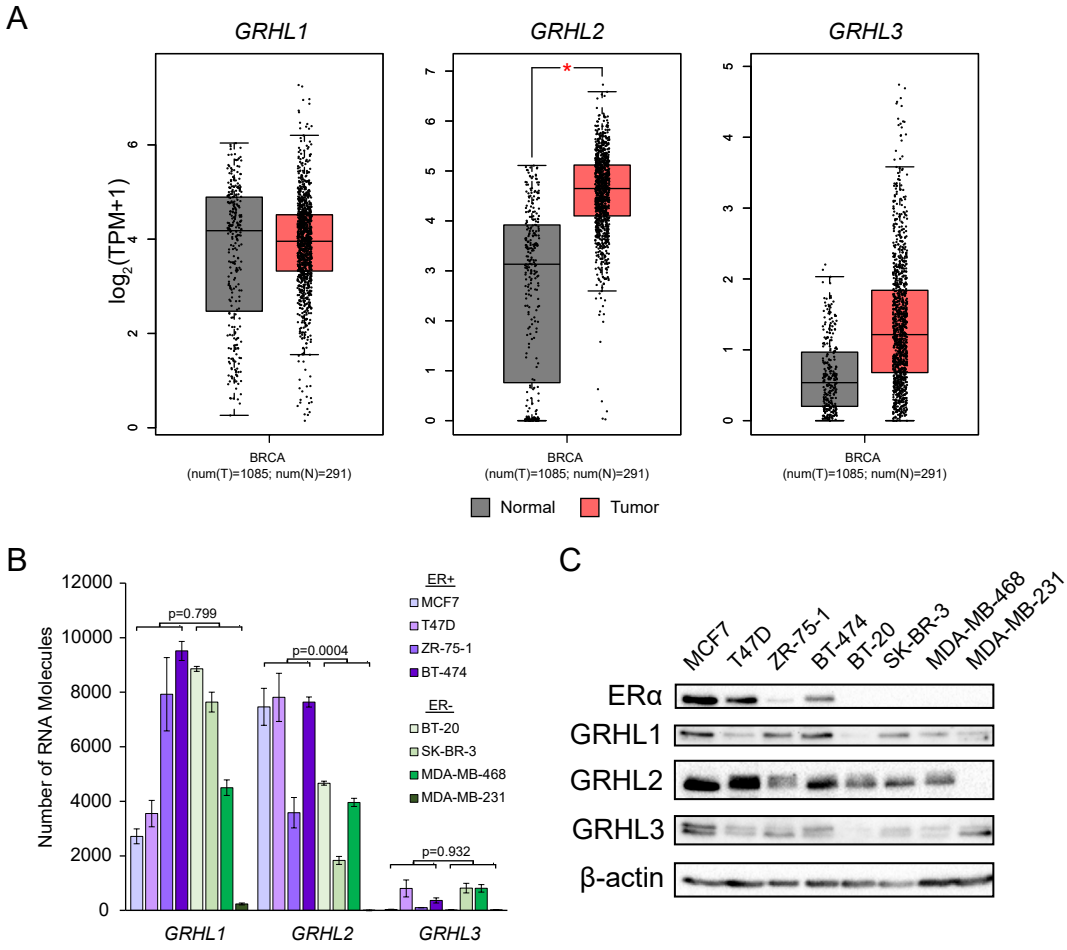

Figure 1: GRHL2 expression is higher in ER-positive vs ER-negative breast cancer. A) mRNA expression of the GRHL family in normal and tumor breast tissue obtained from GEPIA2. A * indicates a p-value < 0.05. B) Absolute quantification of GRHL mRNA and in a panel of ER-positive and ER-negative breast cancer cell lines. Error bars represent mean ± standard error. C) Representative Western blot of GRHL protein levels in the same cell panel. β-actin is used as a loading control.

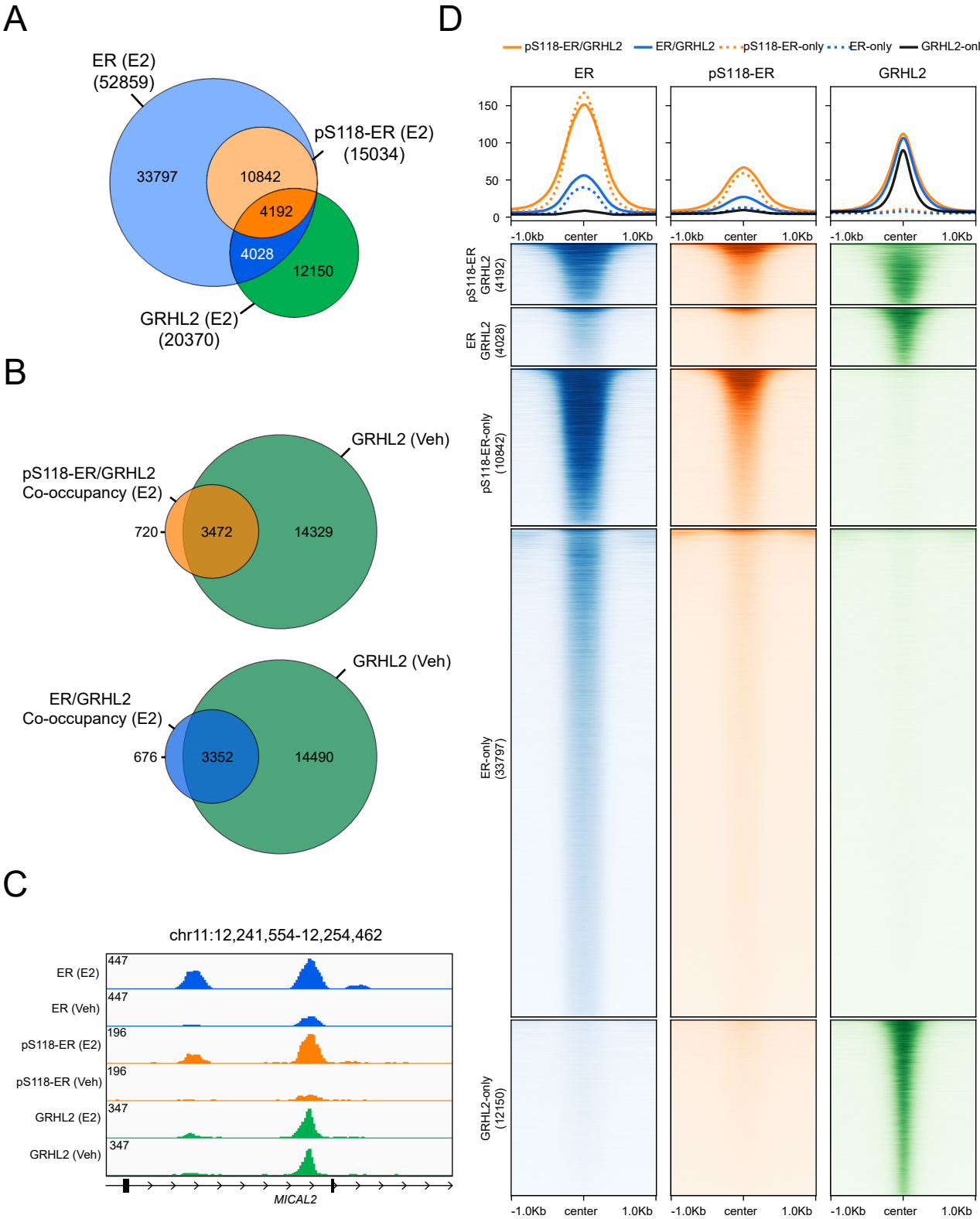

Figure 2: Identification of pS118-ER/GRHL2 co-occupancy sites. A) Venn diagram showing the overlap of MCF7 E2-treated total ER, pS118-ER, and GRHL2 ChIP-seq datasets. pS118-ER binding sites are a subset of total ER bindings sites. ER sites are defined as those that do not overlap with the pS118-ER dataset. Five binding categories were established: pS118-ER/GRHL2 co-occupancy (4,192 sites), ER/GRHL2 co-occupancy (4,028 sites), pS118-ER-only (10,842 sites), ER-only (33,797 sites), and GRHL2-only (12,150 sites). B) Venn diagrams showing the overlap of pS118-ER/GRHL2 co-occupancy sites and ER/GRHL2 co-occupancy sites with GRHL2 peaks detected in vehicle conditions. C) Representative genome browser track of a pS118-ER/GRHL2 co-occupancy site. D) Heatmaps showing binding signal of ER, pS118-ER, and GRHL2 at each of the five binding categories. Data were obtained from previously published ChIP-seq datasets (56).

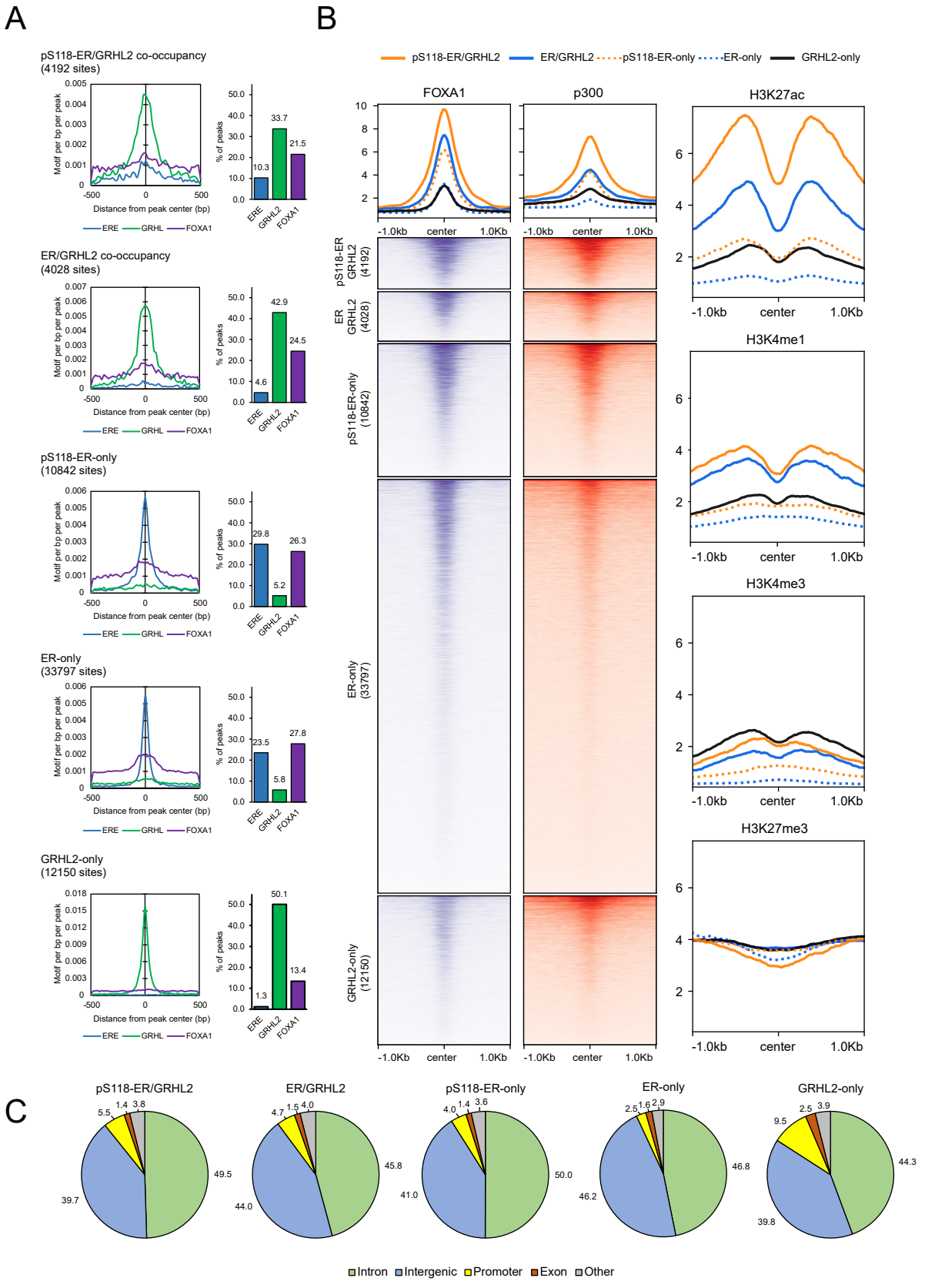

Figure 3: pS118-ER/GRHL2 co-occupancy sites are located at enhancers. A) Motif analysis of the GRHL, ERE, and FOXA1 motifs at co-occupancy sites. The first column shows enrichment of the indicated motif (ERE in blue, GRHL in green, FOXA1 in purple) relative to the peak center. The second column shows the percent of sites with each of the motifs. C) Heatmaps showing binding signal of FOXA1 and p300 and metaplots showing the signal of the histone modifications H3K4me1, H3K4me3, H3K27ac, and H3K27me3 at each of the previously established binding categories. Data were obtained from previously published ChIP-seq datasets (82-85). C) Genome location annotation of the five binding categories. Sites were annotated to introns, intergenic regions, promoters, exons, or other. Promoters were defined as -1kb to +100bp from the transcription start site.

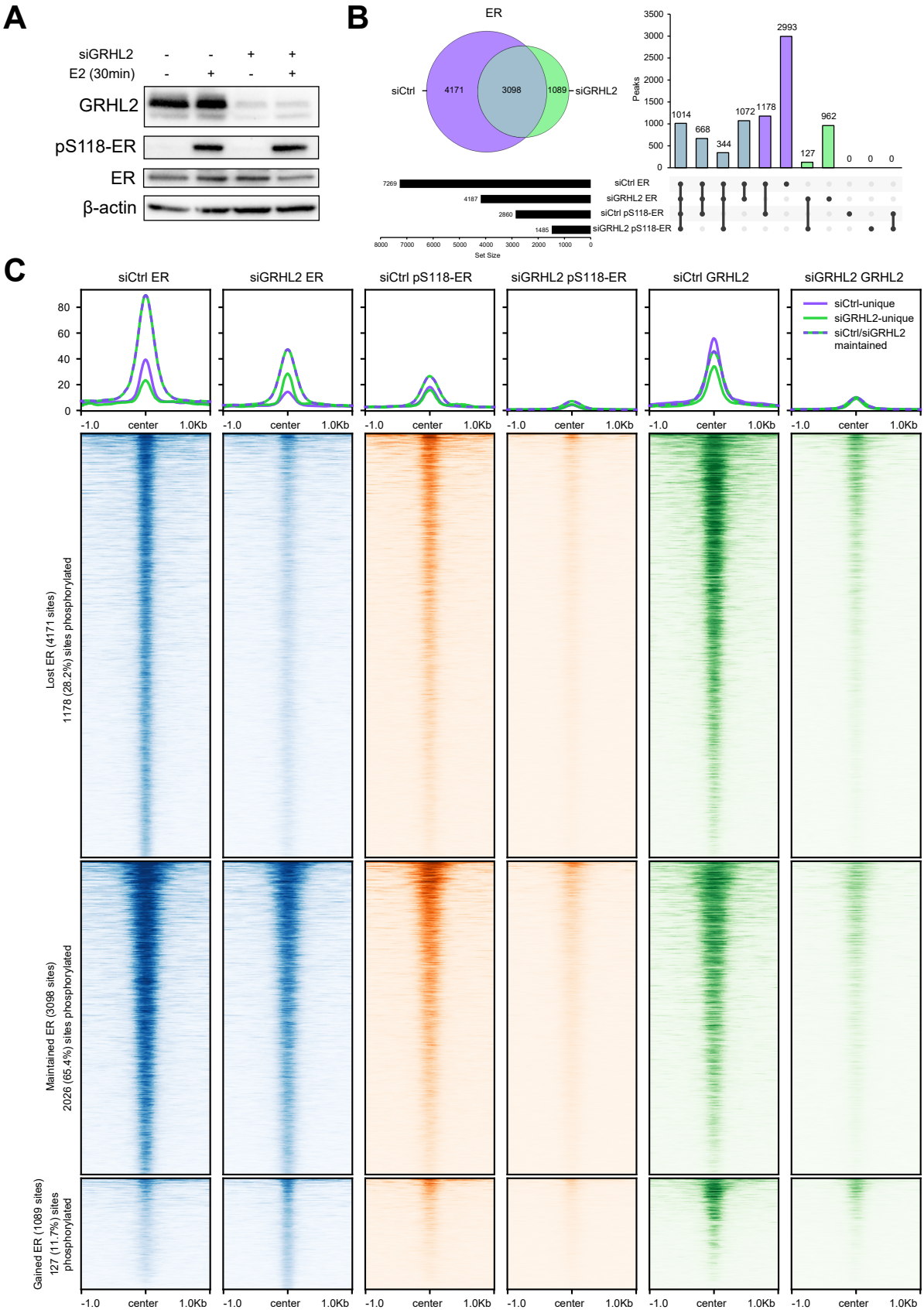

Figure 4: The loss of GRHL2 causes a reduction in ER and pS118-ER chromatin binding. A) Representative western blot of MCF7 samples used in CUT&RUN experiments. Cells were transfected with siCtrl or siGRHL2 and treated for 30 minutes with vehicle or 10 nM E2. β-actin is used as a loading control. B) Venn diagram and upset plot indicating the overlap of ER and pS118-ER CUT&RUN peaks in E2-treated, siCtrl- or siGRHL2-transfected cells. C) Heatmaps showing CUT&RUN signal for ER, pS118-ER, and GRHL2 at lost ER sites (purple), maintained ER siCtrl/siGRHL2 sites (purple and green dashed), and gained ER sites (green). The percent of ER sites detected by the pS118-ER antibody are indicated in region labels.

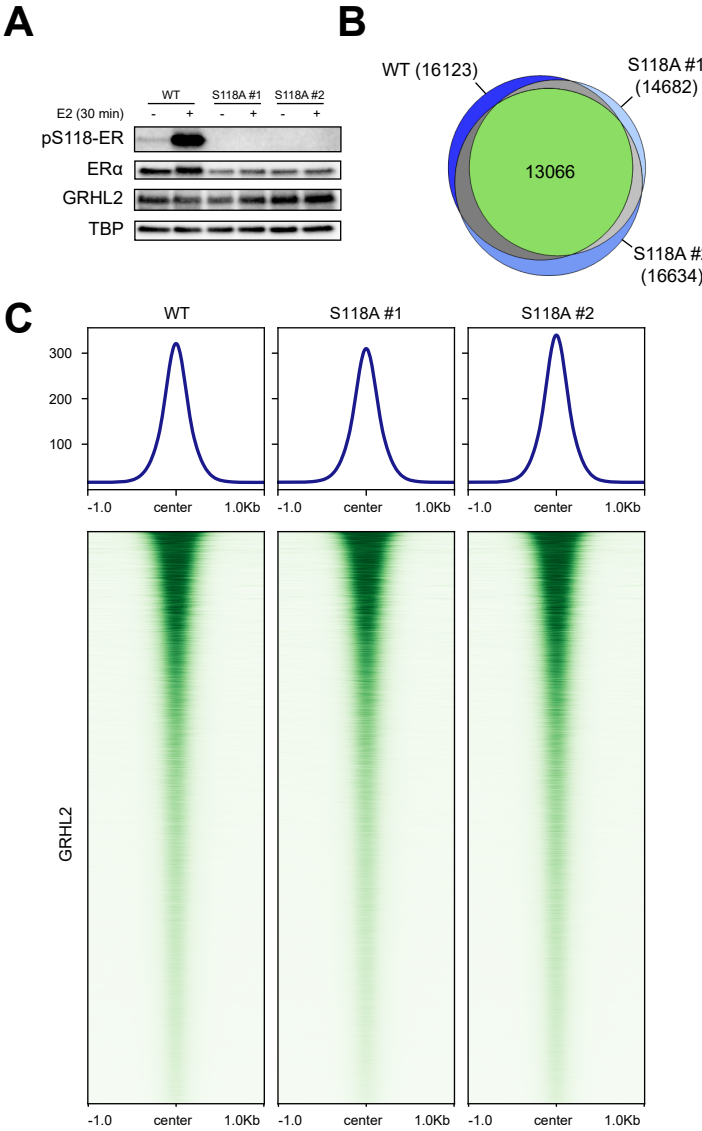

Figure 5: Loss of pS118-ER does not affect GRHL2 chromatin binding. A) Representative western blot of WT and S118A mutant MCF7 cells used for ChIP-seq. Cells were treated for 30min with vehicle or 10 nM E2. TBP is used as a loading control. B) Venn diagrams showing the overlap of E2 GRHL2 binding sites between WT cells and two S118A mutant clones. C) Heatmaps showing GRHL2 binding signal at collective GRHL2 binding sites across all three cell lines.

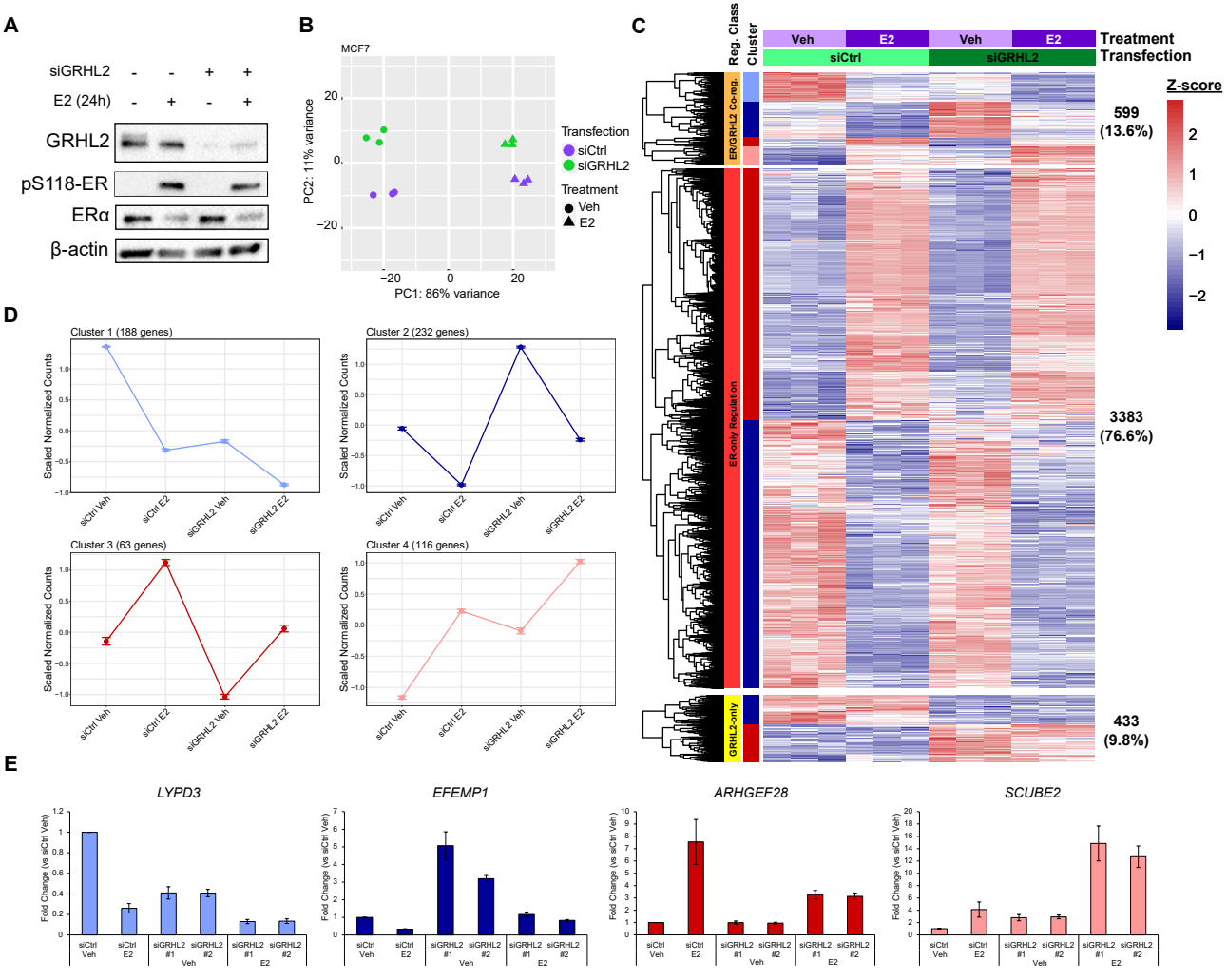

Figure 6: GRHL2 can enhance and antagonize E2-mediated ER transcriptional activity. A) Representative Western blot of MCF7 samples used in RNA-seq. Cells were transfected with siCtrl or siGRHL2 and treated for 24 hours with vehicle or 10 nM E2. β-actin is used as a loading control. B) PCA plot of MCF7 RNA-seq data displaying differences between siCtrl (purple), siGRHL2 (green), vehicle treatment (circles), and E2 treatment (triangles). C) Heatmap showing the expression of ER/GRHL2 co-regulated genes, ER-only regulated genes, and GRHL2-only regulated genes. D) Gene expression profiles of ER/GRHL2 co-regulated gene clusters. Error bars represent mean ± standard error. E) qPCR validation of selected genes from each of the ER/GRHL2 co-regulated gene clusters using two different siRNAs against GRHL2. All values are relative to siCtrl Veh. Error bars represent mean ± standard error.

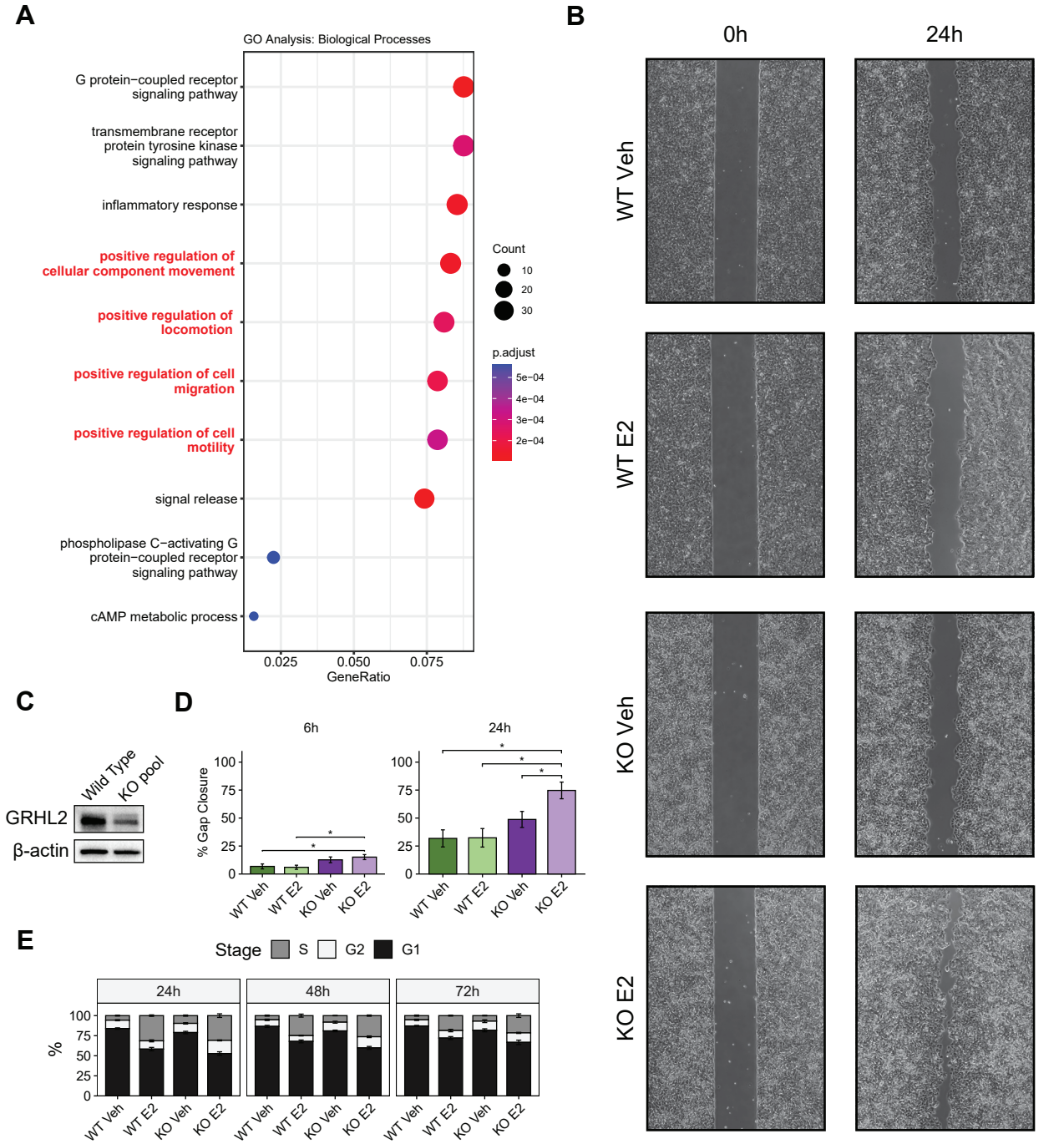

Figure 7: GRHL2 and E2 co-regulate migration. A) Gene ontology analysis for biological processes performed with clusterProfiler on ER/GRHL2 co-regulated genes. Terms related to cell migration, motility, and locomotion are highlighted in red. The size of the dots represents the number of genes annotated to a given term, and color represents the adjusted p-value with red being the most significant. B) Brightfield images of WT and GRHL2-KO cell migration across a cell-free gap over the course of 24 hours. C) Representative Western blot showing the loss of GRHL2 in pooled CRISPR GRHL2-KO cells. D) Quantification of the percent gap closure over 6 hours and 24 hours. Error bars represent mean ± standard error and * indicates a p-value < 0.05. E) Flow cytometry analysis showing the percent of cells in each of the cell cycle stages (S, G2, G1). WT and GRHL2-KO cells were treated with vehicle or 10 nM E2 over 24h, 48h, and 72h. Error bars represent mean ± standard error.

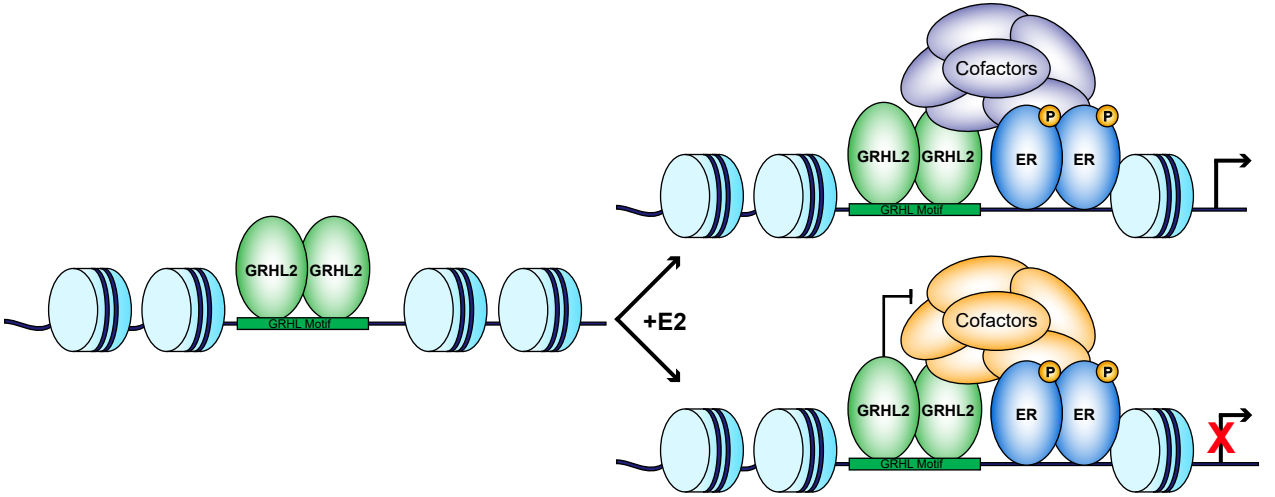

Figure 8: Model of GRHL2 function in facilitating pS118-ER binding and transcriptional activity. GRHL2 binds to the GRHL motif in enhancers prior to ligand treatment. Upon exposure to E2, GRHL2 can either promote gene transcription by facilitating the recruitment of coregulators like MLL3, or repress gene transcription by repressing coregulators, like p300.